Catalysis Today 437 (2024) 114777

Contents lists available at ScienceDirect

Catalysis Today

journal homepage: www.elsevier.com/locate/cattod

Catalytic CO_2 hydrogenation to hydrocarbon fuels in a potassium ion-conducting reactor

Esperanza Ruiz [a,*], María Villuendas [b], Ángel Morales [a], Meryem Farchado [a], José María Sánchez [a]

[a] Centro de Investigaciones Energéticas, Medioambientales y Tecnológicas (CIEMAT), Av. Complutense, 40, Madrid 28040, Spain
[b] Material Science Department, Escuela Técnica Superior de Ingenieros de Caminos, Canales y Puertos (ETSICCP), Universidad Politécnica de Madrid, C/ Profesor Aranguren, 3, Madrid 28040, Spain

ARTICLE INFO

Keywords:
Electrochemical promotion
CO_2 hydrogenation
Fe/K-β-Al_2O_3
Potassium
Hydrocarbons

ABSTRACT

The electrochemically assisted CO_2 hydrogenation directly to hydrocarbon fuels was studied, apparently for the first time, over a cheap, widespread and non-precious Fe catalyst in a potassium ion conducting (K-β-Al_2O_3) reactor, under atmospheric pressure, at relatively low temperatures and using representative concentrated CO_2 and H_2 gas mixtures and an easily scalable tubular catalyst-electrode configuration. The Fe electrocatalytic film was deposited by dip-coating on a commercial K-β-Al_2O_3 candle and characterized, both as prepared and after activation and testing, by TPR, TGA, XPS, XRD and SEM-EDX. The optimum operating conditions for both Fe activation (300 ºC, 75% H_2, 24 hours) and electropromoted CO_2 hydrogenation (300 ºC, 1.5 V, H_2/CO_2=3) were identified. Long-term tests on electrochemically promoted CO_2 hydrogenation to hydrocarbons were performed under selected operating conditions to assess electrocatalyst stability. Both the selectivity to the target product (C_{5+} hydrocarbons) and the stability of the catalyst can be tuned in situ by modifying the potassium surface coverage via electrochemical pumping of potassium ions through the applied polarization. Finally, as an attempt to improve the catalyst-electrode behaviour, powdered catalysts, based on iron nanoparticles dispersed on KVO_3 (a K^+ and e^- co-conductor) with different Fe loadings (17 and 9 wt%) were prepared and comparatively studied for CO_2 hydrogenation to hydrocarbons. The catalyst with higher Fe loading was selected as the most promising, in terms of activity, selectivity and stability, for further catalyst-electrode optimisation by deposition, via dip-coating, of a Fe-KVO_3 film on the K-β-Al_2O_3 candle.

1. Introduction

CO_2 hydrogenation to hydrocarbon fuels is considered a strategy to diminish greenhouse gas emissions and reliance on fossil sources while storing the renewable energy needed for the electrolytic H_2 production and CO_2 conversion processes through the so-called Power to Fuel (PtF) technology [1,2]. CO_2 hydrogenation to hydrocarbons is considered as a modification of the traditional Fischer-Tropsch process for the synthesis of hydrocarbons from syngas, a mixture of CO and H_2, generated via Reverse Water Gas Shift (RWGS) reaction in a separated reactor [3].

CO_2 can be directly converted to hydrocarbons, as reported in literature [4,5], over Fe supported catalysts, which are active for both RWGS and Fischer-Tropsch reactions, via the CO_2 hydrogenation reaction (1).

$$n\,CO_2 + (3n+1)\,H_2 \rightarrow C_nH_{2n+2} + 2n\,H_2O \quad (1)$$

Direct CO_2 hydrogenation to hydrocarbons consists of two consecutive reactions: an initial reduction of CO_2 to CO through RWGS reaction (2) followed by CO conversion to hydrocarbons via and the Fischer-Tropsch synthesis reaction (3). Both reactions occur on the active centres of the Fe catalyst [6–8].

$$CO_2 + H_2 \rightarrow CO + H_2O \quad (\Delta Hr = +40 kJ/mol) \quad (2)$$

$$n\,CO + (2n+1)\,H_2 \rightarrow C_nH_{2n+2} + n\,H_2O \quad (3)$$

Methanation (4−5), oxygenates (alcohols or ethers) synthesis (6) and Boudouard (7) side reactions, which affect catalyst selectivity and stability, can also take place:

$$CO_2 + 4\,H_2 \rightarrow CH_4 + 2\,H_2O \ (\Delta Hr = -165 kJ/mol) \quad (4)$$

* Corresponding author.
E-mail address: esperanza.ruiz@ciemat.es (E. Ruiz).

https://doi.org/10.1016/j.cattod.2024.114777
Received 28 February 2024; Received in revised form 26 April 2024; Accepted 28 April 2024
Available online 6 May 2024

$$CO + 3\,H_2 \rightarrow CH_4 + H_2O \quad (\Delta Hr = -206 kJ/mol) \tag{5}$$

$$x\,CO_2 + (2x - z + y)\,H_2 \rightarrow C_xH_yO_z + (2x - z)\,H_2O \tag{6}$$

$$2CO \rightarrow CO_2 + C \quad (\Delta Hr = -173 kJ/mol) \tag{7}$$

To produce fuels (branched chain hydrocarbons), a third isomerization reaction (8) is needed, in which the straight chain hydrocarbons resulting from the Fischer-Tropsch synthesis reaction are transformed into branched hydrocarbons on the acid sites of the support [9–11].

$$C_nH_{2n+2} \rightarrow Iso - C_nH_{2n+2} \tag{8}$$

However, the product distribution can be wide depending on catalyst structure and composition [9]. Hydrocarbons products mainly consisted in low molecular weight hydrocarbons (paraffins and olefins) instead of C_{5+} products that are more valuable as liquid transportation fuels [12,13]. Different types of promoters, such as second metals (Cu, Ru, Co), alkaline metals (Na, K) and acidic metal oxide supports (Al_2O_3, SiO_2, TiO_2) can be employed to tune the product distribution towards heavier hydrocarbons [12]. According to literature, the combination of Fe, K and alumina results in a strong metal-support interaction which makes the catalyst highly active and selective for CO_2 hydrogenation to long chain hydrocarbons [14,15].

Multifunctional alumina supported Fe based catalysts chemically promoted with potassium are reported to be active and selective for CO_2 hydrogenation to long-chain hydrocarbons (C_{5+}) in one step, by matching of RWGS, over Fe_3O_4 sites, C-C coupling, over Fe_5C_2 sites, and isomerization, over acid sites of the support [9].

Adding potassium promoter during Fe based catalyst preparation procedure (chemical promotion) can tailor the hydrogen and carbon coverage on the catalyst surface, which play an important role in altering product distribution in CO_2 hydrogenation [16,17].

Potassium promoter can be also electrochemically added in-situ to the catalyst surface during the CO_2 hydrogenation process (electrochemical promotion), tailoring surface coverage of H and C by controlling K pumping (i.e. K surface coverage) via modification of the applied potential, and, therefore, enabling to tune hydrocarbon product distribution to the desired fuel like fraction [18,19]. Therefore, electrochemical promotion of catalysis (EPOC) may allow the increment of the catalytic activity for the CO_2 hydrogenation reaction and altering the selectivity to the desired products, such as C_{5+} hydrocarbons based fuels, with the potential to improve energy efficiency and reduce the costs of the process [20–22]. In fact, the application of small currents or potentials between an electrical conductive metal/metal oxide catalyst which is in contact with an ion conducting (e.g. K^+) solid electrolyte, and a counter electrode results in the moving of promoting species (e.g. K^+ ions) to the catalyst surface, allowing in-situ modification of the relative chemisorption between the different coexistent reaction gases (e.g. CO_2, H_2), which result in a pronounced increment of catalytic activity and selectivity to the desired products (e.g. C_{5+} hydrocarbons) [23].

The RWGS reaction can be electrochemically promoted, at low temperature, by sodium [24–27] and potassium [26–29]. The electrochemically promoted RWGS reaction has been also studied over Fe based catalyst supported on YSZ (an O^{2-} promoter conductor) [30–33].

From the best of the authors knowledge, there are only three studies in literature dealing with the electrochemical promotion of CO based Fischer-Tropsch synthesis reaction (3) by potassium [18,19] on Rh or by sodium on Ru [34], which confirmed the possibility of applying EPOC to a C–C bond forming reaction. It seems that electro-pumping of K to the catalyst surface increases the probability of chain growth while supressing methanation reaction, with sustained increase in selectivity to higher hydrocarbons as the alkali loading is increased [18,19]. However, from the best of the authors knowledge, the electrochemical promotion with potassium of the one-step CO_2 hydrogenation directly to long-chain hydrocarbons (1) has not been studied so far. In addition, most of these studies have been carried out using reactor configurations (discs) [24–33], costly metals (Pd, Ru, etc.) [24–26,28], metal film preparation methods [24–33] and simplified gas compositions (H_2 and CO_2 diluted in He or N_2) [24–26,28–33] which are not representative of the potential practical application of the technology. The electrochemical promotion of catalytic CO_2 hydrogenation to oxygenated and light hydrocarbons (CH_3OH, DME, CH_4, etc.) has been recently studied, over cheap (based on Fe, Cu, Ni) and easily scalable electrocatalyst configurations (coated solid oxide electrolyte tubes) and under realistic conditions at bench scale, by our research group [35–39].

Given that electrocatalyst films should be electrical conductive and continuous to allow system polarization, the main disadvantage of the EPOC technology is the low catalytic activity per mass unit, resulting from the low metallic dispersion and surface area of typical catalyst-electrodes versus those of conventional heterogeneous catalysts (metallic dispersion up to 40%) [40]. Therefore, additional research is needed for improving efficiency, selectivity, stability and durability of electrocatalysts.

This work presents, to the extent of our knowledge for the first time, a study of the electrochemically assisted CO_2 hydrogenation directly to hydrocarbons over a cheap, widespread and non-precious Fe catalyst, in a potassium ion conducting (K-β-Al_2O_3) reactor and using operating conditions, such as atmospheric pressure, relatively low temperatures and concentrated CO_2 and H_2 gas mixtures, and an easily scalable tubular catalyst-electrode configuration, which are more representative of the potential practical application of the technology.

In this work, we propose the application of the Electrochemical Promotion of Catalysis (EPOC) to the direct CO_2 hydrogenation to hydrocarbon fuels. The objective of this work is the development and study of easily scalable (tubular) configurations of multifunctional Fe based electrocatalysts for the synthesis of hydrocarbons via electrochemically promoted CO_2 hydrogenation. This work also aims at the optimization of the design and preparation techniques of the Fe catalyst-electrode film in order to increase electronic and ionic conductivity and metal-support interactions and dispersion and to provide additional acid sites for isomerization.

2. Material and methods

2.1. Catalyst preparation

2.1.1. Fe/K-β-Al_2O_3/Au electrochemical catalyst

The electrochemical catalyst evaluated in the present work consisted of a thin Fe film (catalyst-working electrode), coated on the outer surface of a 28-mm-i.d., 100-mm-long, and 1–2 mm-thick K-β-Al_2O_3 tube, closed flat at one end (IONOTEC).

A gold counter electrode was deposited on the internal side of the K-β-Al_2O_3 candle to carry out polarizations. Au was selected as electrode material given that it is reported [41,42] to be inert for the CO_2 hydrogenation reaction. The Au counter electrode was prepared by applying a thin layer of gold paste (HERAEUS-C5729) and subsequent drying at 150 °C and annealing at 850 °C during 10 min (heating ramp of 15 °C/min) [24].

Then, the iron catalyst film was deposited by “dip-coating” on the external side of the solid electrolyte candle. The opened end of the K-β-Al_2O_3 candle was capped to prevent active catalyst particles from being added to the counter electrode side. Firstly, the substrate was cleaned with absolute ethanol in an ultrasonic bath, rinsed with absolute ethanol and dried in an oven at 90 °C during 30 minutes. Then, iron oxide (hematite) was deposited by dip-coating, withdrawing the substrate from a precursor solution composed of 2-(2-aminoethylamino) ethanol, ethanol and ferrous nitrate [43], at a speed of 10 cm/min. After that, the coating was thermally cured at 500 °C during 60 minutes and then in-situ activated using a previously optimized procedure, which consisted on reducing the obtained Fe-film in a stream (1500 NmL min^{-1}) of 75 vol% H_2 in He at 300 °C during 24 h (with a heating ramp

of 5 ºC min^{-1}), in order to transform the as deposited hematite (Fe_2O_3) phase into the magnetite (Fe_3O_4) phase active for Reverse Water Gas Shift (RWGS) reaction.

2.1.2. Powdered iron based catalysts

Powder of the same iron phase (Fe_2O_3) as in the as deposited electro-catalytic film was prepared by heating the precursor solution at 200 ºC to remove ethanol and organic matter, resulting in the formation of an iron crust. The iron crust was then calcined at 500 °C for 1 hour and pulverized to obtain hematite powder (Fe_2O_3).

A powdered catalyst, based on iron nanoparticles (Sigma Aldrich), with 35 nm in average size and 99.5% Fe in purity, dispersed on potassium metavanadate (Sigma Aldrich) (KVO_3), a K^+ and e^- co-conductor, with two different Fe loadings (17 and 9 wt%), were prepared as candidate electrode material to improve the dispersion and the ionic and electronic conductivity of the Fe electro-catalyst film. The Fe loading range was selected to avoid the potential decrease in dispersion associated with the formation of iron agglomerates [13] while enabling the assessment of the potential loss in catalytic performance resulting from potassium overloading of the catalyst surface [44,45].

The Fe-KVO_3 powder was prepared from a precursor solution consisting of potassium metavanadate (KVO_3), 2-(ethylamino)-ethanol and the corresponding amount of iron nanoparticles according to the required Fe content. The precursor solution was heated to 200 ºC to remove ethanol and organic matter and calcined at 500 ºC for 1 h to obtain the iron hematite phase.

2.2. Catalyst characterisation

2.2.1. Fe/K-β-Al_2O_3/Au electrochemical catalyst

The cross-section and the outer surface (Fe film) of the Fe/K-β-Al_2O_3/Au electrochemical cell were characterised, both as prepared (after Fe deposition and calcination in air), after reduction and after testing, by Scanning Electron Microscopy (SEM) coupled to Energy Dispersive X-ray spectroscopy (EDX), X-Ray Diffraction (XRD) and X-ray Photoelectron Spectroscopy (XPS) techniques.

The morphology, thickness and surface Fe distribution of the iron film were examined via SEM-EDX by means of a HITACHI SU6600 FEG-SEM instrument with ZrO/W emission type of 1 kV - 30 kV (100 V steps) of accelerating voltage and 3 nm - 1.2 nm of resolution.

Diffractograms of the Fe film were recorded on a PHILIPS "Xpert-MPD" apparatus utilizing a Cu Kα X-ray source (40 mA and 45 kV), a step time of 2 s, a 2θ range of 15–75º and a step size of 2θ=0.03º. XRD patterns of the Fe film were recorded on a X'PERT PRO PANALYTICAL diffractometer. Measures were performed at 2θ range of 2–100º, using CuKα radiation (λ= 1.540598 Å) and removing Kβ radiation by a nickel filter, with a 0.05 ° s^{-1} scanning, and an accumulation time of 2 s. Crystalline phases were identified by X'PERT HIGHSCORE PLUS software, comparing the patterns obtained to PDF-2 data base of the Joint Committee on Powder Diffraction Standards JCPDS.

The surface chemical composition of the Fe film was analysed via XPS by a Perkin-Elmer PHI 5400 System with a beam diameter of 1 mm and a Mg Kα ($h\nu$ = 1253.6 eV) excitation source (20 mA and 15 kV). Base pressure in the analytical chamber was about 10^{-9} Torr. The step energy was 89.5 eV for broad spectra (0–1100 eV) and 35.75 eV for high resolution spectra. The energy scale was referenced to the carbon 1 s signal at 285.0 eV.

2.2.2. Powdered iron oxide catalyst

The as prepared Fe_2O_3 powder was characterised by TPR (Temperature Programmed Reduction) and TGA (Thermal Gravimetric Analysis) in order to propose an effective electro-catalyst activation procedure via reduction of the as-prepared Fe_2O_3 film to the active phase (Fe_3O_4) for the Reverse Water Gas Shift (RWGS) reaction.

TPR experiments were performed in a quartz tubular reactor (6 mm O.D.) where the catalyst sample was placed between two quartz wool plugs. The reactor is heated by an electrical furnace having low heating inertia. The reactor is coupled with a gas micro-chromatograph (micro-TCD), described in detail elsewhere [35,38], for on-line monitoring of the reduction process. Bronkhorst Hi-Tech mass flow controllers were used to produce synthetically and feed the reducing gas mixture. Gas temperature is controlled and recorded versus time.

100 mg of Fe_2O_3 powder sample was introduced in the reactor and outgassed in a 100 NmL·min^{-1} He stream at 300 ºC for 1 h, and then cooled in He flow down to 25 ºC. After that, a stream of 100 NmL·min^{-1} of 4%vol H_2 in He was fed to the reactor, while heating the sample up to 650 ºC at a heating rate of 5 ºC·min^{-1}.

In order to get deeper insight into reduction of hematite, thermal analysis system TGA 2 (Mettler Toledo Corporation, Switzerland) was used to measure hematite mass variation versus temperature under CO and H_2 reductive atmospheres. 10 mg of Fe_2O_3 powder sample was placed in an alumina crucible avoiding contact with both sides of the oven. Before performing any analysis, temperature, weight, and platform calibrations were carried out.

In the case of H_2-TPR, the Fe_2O_3 powder sample was outgassed in a 50 NmL·min^{-1} N_2 flow at 300 ºC for 1 h, and then cooled in N_2 flow down to 25 ºC. After that, a stream of 50 NmL·min^{-1} of 4%vol H_2 in N_2 was fed to the reactor while heating the sample up to 700 ºC at a heating rate of 5 ºC·min^{-1}.

In the case of CO-TPR, a stream of 50 NmL·min^{-1} of 5%vol CO in N_2 was fed to the reactor while stepwise heating the sample from 25 ºC to 200 ºC at a heating rate of 10 ºC·min^{-1}, and then from 200 ºC to 700 ºC at 2.5 ºC min^{-1}.

2.3. Experimental set-up

Electrochemically assisted CO_2 hydrogenation over the Fe catalyst film was studied in a bench-scale plant described in detail elsewhere [38], which operates at atmospheric pressure and up to 900 ºC. The Fe/K-β-Al_2O_3/Au electrochemical catalyst was placed in a fixed-bed down-flow quartz reactor. Both catalyst (Fe) and counter (Au) electrodes were connected to a potentiostat-galvanostat (Voltalab 21) through inert gold wires (HERAEUS), to assure that any voltage potential-induced variation in catalytic activity and selectivity can be solely ascribed to the Fe catalyst film.

Conventional catalytic CO_2 hydrogenation over both Fe_2O_3 and Fe-KVO_3 powdered catalysts was also studied at lab-scale in a Microactivity Pro Unit, which is able to operate up to 650 ºC and 25 bar, described in detail elsewhere [46,47]. The powdered samples were placed in a fixed-bed down-flow stainless steel tubular reactor heated by a single zone electric furnace.

In both cases, H_2, CO_2 and N_2 bottled gases (Air Liquide) were metered by a battery of electronic mass flow controllers (Brokhorst High-Tech). The sampling lines from the reactor exit to the gas analysis system were heated to avoid any possible product condensation. Gas samples were analysed by a gas micro-chromatograph (Varian CP-4900), described detail elsewhere [35,38], enabling the analysis of H_2, N_2, CO, CH_4, CO_2 and light hydrocarbons and oxygenates, and by a 5890 Series II Hewlett-Packard gas chromatograph, equipped with a flame ionization detector (FID), which allowed quantitative analysis of heavier hydrocarbon compounds calibrated from different Alphagaz PIANO calibration standards (Sigma-Aldrich).

2.4. Operating conditions and procedure

Before performing each electrochemically assisted CO_2 hydrogenation experiment, the iron film was subjected to an additional reduction pre-treatment, under specific operating conditions (1500 NmL min^{-1} of 75 vol% H_2 in N_2 at 300 ºC during 1 hour), in order to reduce the potential Fe_2O_3 formed by re-oxidation of Fe_3O_4 in preceding tests.

After that, a series of comparative tests was carried out to select the most appropriate operating conditions for the electropromoted CO_2

hydrogenation process.

A positive potential of 3 V was applied between the Fe and the Au electrodes during 30 min prior to each test in order to clean the Fe catalyst surface from potassium ions, which could thermally migrate to the catalyst surface, and to ensure the decomposition of any potential adsorbed species, as a way to define a reproducible reference state (unpromoted state) of the Fe catalyst surface.

The first series of experiments were performed, using a highly demanding gas flowrate (1500 NmL min^{-1}), both under temperature programmed and potentiostatic modes, by following the effect of temperature (between 200 and 400 ºC) at 3 V (unpromoted conditions) and applied potential (between 3 and −2.5 V) at the temperature selected from the temperature programmed tests, respectively, on CO_2 conversion and selectivity to the different products.

Additional tests were carried out under unpromoted conditions at the temperature selected from the temperature programmed tests and using different gas flowrates (between 150 and 1500 Nml min^{-1}) to determine the influence of gas flowrate on CO_2 conversion and selectivity to the different products and to assure that the previous tests were carried out under conditions of global reaction rate limiting-chemical kinetics, i.e., in the absence of mass transfer limitations at the gas-solid interface.

Once the most appropriate operating conditions for the electropromoted CO_2 hydrogenation were identified, various long-term (up to 48 hours) tests were carried out to assess catalyst stability and to identify potential deactivation phenomena, such as carbon deposition, sintering or active phase re-oxidation, which may result in a diminution of catalytic activity and selectivity to hydrocarbons. These tests also enabled to determine whether the electrocatalyst can be activated for the Fischer-Tropsch synthesis, via formation of the corresponding active phase (iron carbide) through carburization of the magnetite by the CO formed via the RWGS reaction.

Both, Fe_2O_3 and Fe-KVO_3, powdered catalysts were as well pre-reduced in a stream (340 NmL min^{-1}) of 75 vol% H_2 in N_2 at 300 ºC during 24 hours. According to literature [13], the long-term catalytic CO_2 hydrogenation tests were carried out at 300 ºC and 13.5 bar using a GHSV (Gas Hourly Space Velocity) of 1400 h^{-1}.

All, electropromoted and conventional, CO_2 hydrogenation tests were performed under H_2 and CO_2 binary mixtures with a stoichiometric H_2/CO_2 molar ratio of 3, which thermodynamically favours the synthesis of hydrocarbons from CO_2. Although a small amount of N_2 was added to the reaction gas mix as an internal standard.

CO_2 conversion (X_{CO_2}), "CO_2 free selectivity" (S_i) and the catalytic rate of CO_2 conversion (rCO_2) and product formation (r_i) were calculated as follows [39]:

$$X_{CO_2} = \left(1 - \frac{[CO_2]_o \times [N_2]_i}{[CO_2]_i \times [N_2]_o}\right) * 100 \quad (9)$$

Where $[CO_2]_i$ and $[CO_2]_o$ and $[N_2]_i$ and $[N_2]_o$ are the inlet and outlet CO_2 and N_2 molar concentrations.

$$S_i = \left(\frac{c_i * M_i}{\sum_{j=1}^{j=np} c_j \times M_j}\right) * 100 \quad (10)$$

Where "S_i" is the selectivity, "c_i" is the number of carbon atoms and "M_i" is the molar flow of product i, respectively, and "np" is the number of different products formed.

$$rCO_2 = \frac{(Q_{CO_2} * X_{CO_2})/100}{22414 * 60} \quad (11)$$

Where rCO_2 is the rate of CO_2 conversion in mol/s, Q_{CO_2} is the CO_2 flowrate in NmL/min, and 22414 is the molecular volume of a gas in NmL/mol.

$$r_i = \frac{rCO_2 * S_i}{100} \quad (12)$$

Where, r_i is the catalytic rate of formation of product i in mol/s and rCO_2 and S_i are obtained from (11) and (10), respectively.

The effect of polarization on catalyst performance for the CO_2 hydrogenation reaction was evaluated in terms of rate enhancement ratio (ρ_i) and NEMCA (Non faradaic Electrochemical Enhancement of Catalytic Activity) enhancement factor (Λ), defined as follows [39]:

$$\rho_i = \frac{r_i}{r_{io}} \quad (13)$$

$$\Lambda_i = \frac{(r_i - r_{io}) * E_i}{I/F} = \frac{\Delta r_i * E_i}{I/F} \quad (14)$$

Where r_i is the electropromoted rate (under a given applied potential V) and r_{io} is the unpromoted catalytic rate (under application of 3 V) of the corresponding product formation. F is the constant of Faraday (96485 C/mol), I is the applied current, Δr_i is the potential-induced modification in the catalytic rate (mol/s) and E_i is the number of electrons transferred divided by the stoichiometric coefficient in each product formation reaction. Therefore, E_{CH4}=8 and E_{CO}=2.

The total amount of potassium ions electrochemically transferred to the catalyst surface can be determined according to Faraday's law (15) by integration of the current versus time curves obtained for each potential application [35]:

$$molK^+ = \int_0^t \frac{[I]dt}{nF} \quad (15)$$

where n is the potassium ion charge in this case (+1) and t is the polarization time.

3. Results and discussion

3.1. Catalyst characterisation studies

Fig. 1a shows a SEM micrograph of the surface of the as prepared (after Fe deposition and calcination) Fe film.

A SEM micrograph of the interface between the as prepared Fe film and the K-β-Al_2O_3 solid electrolyte is shown in Fig. 1b. The Fe film thickness can be assessed from Fig. 1b and resulted to be around 1 μm.

As can be derived from EDX mappings of the Fe (red) and Al (blue) distribution in the as prepared Fe electrocatalyst in Fig. 2, iron apparently did not penetrate into the K-β-Al_2O_3 solid electrolyte.

Therefore, it can be stated that the developed dip-coating technique allowed the deposition of a thin, porous and fairly well defined iron film.

In Fe-based catalysts, prepared by different procedures that usually include a final calcination step, iron is normally found in the form of hematite (Fe_2O_3) [48]. Therefore, in order to activate the catalyst, a reductive pre-treatment in hydrogen or syngas environments is carried out where, depending on the utilized H_2 concentration and operating temperature [49], hematite undergoes a two or three steps sequential transformation ($Fe_2O_3 \rightarrow Fe_3O_4 \rightarrow FeO \rightarrow Fe$) [50]. Numerous studies have shown that the optimal reduction temperature for obtaining the active phase for the RWGS reaction (magnetite) is between 300 – 400 ºC [51]. However, it has been also reported that the presence of K promoter in the catalyst disfavour H_2 chemisorption and hinders the transformation of Fe_2O_3 to Fe_3O_4 [52].

On the other hand, the active phase for the Fischer-Tropsch reaction of CO (χ-Fe_5C_2) is formed by carburization of the magnetite under CO rich environments during catalyst pre-treatment and/or operation [50]. Furthermore, it has been also reported that the presence of K promoter, which promote C-O bond dissociation, in the catalyst favours also the formation of iron carbide [17,53].

With the aim of identifying the most suitable reduction temperature for the transformation of Fe_2O_3 into Fe_3O_4, temperature programmed reduction (TPR) and thermogravimetric analysis (TGA and DTA) studies were carried out over the as prepared Fe_2O_3 powdered catalyst.

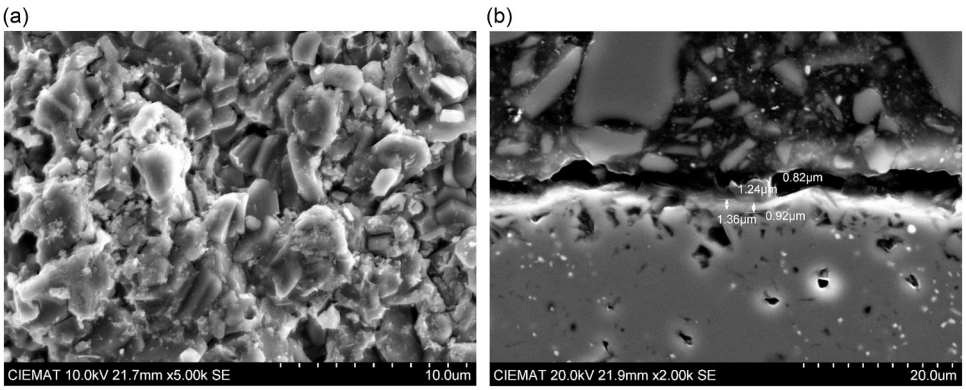

Fig. 1. SEM micrographs of the as prepared Fe film surface (a) and interface (b).

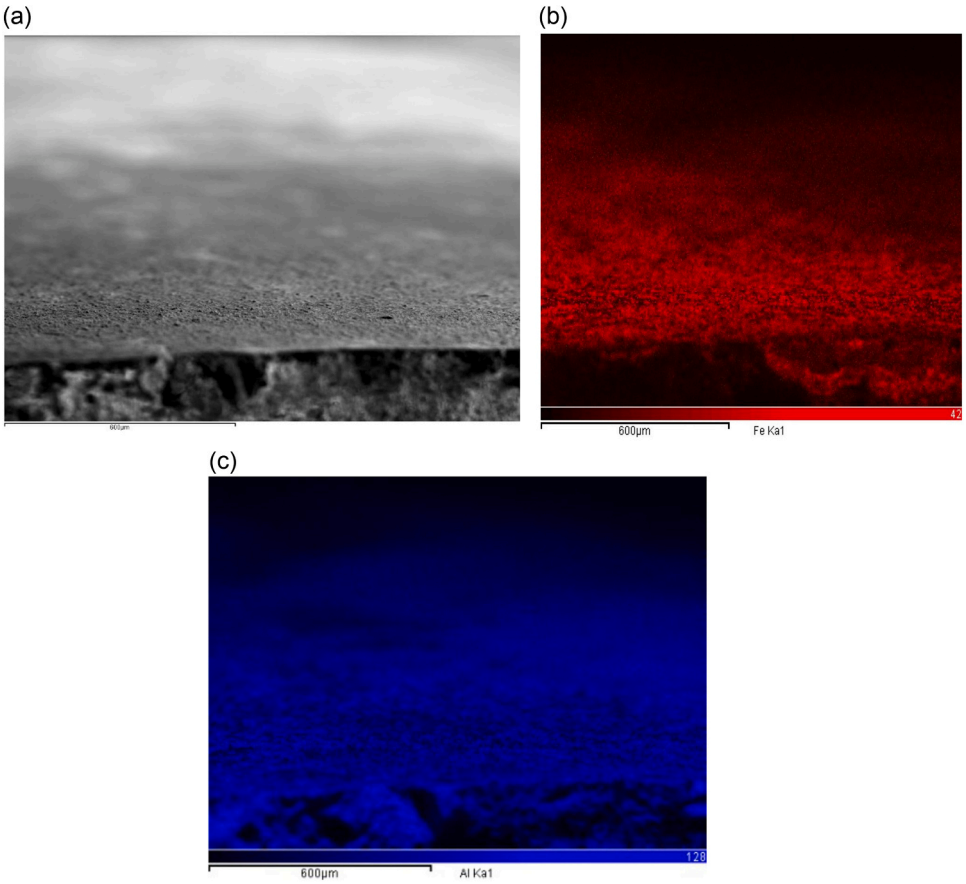

Fig. 2. As prepared Fe electrocatalyst: SEM micrograph (a) and EDX mapping of Fe (b) and Al (c).

Fig. 3 shows the temperature reduction profile of the Fe_2O_3 powdered catalyst. A sharp reduction peak was found at about 350 ºC, which can be assigned to the primary reduction of Fe_2O_3 to Fe_3O_4 [51]. A second broader peak appeared between 500 ºC and 650 ºC, which is attributable to subsequent magnetite (Fe_3O_4) reduction to metallic Fe [49–51].

To gain a deeper insight into hematite reduction, thermogravimetric measurements were also performed under H_2 and CO reducing environments. The obtained TGA-DTA curves are presented in Fig. 4.

Two pronounced mass loss peaks can be observed in Fig. 4a, which, in accordance with TPR-H_2 results, seems to confirm that the hematite reduction process under H_2 atmospheres takes place in two consecutive steps [51]: hematite (Fe_2O_3) to magnetite (Fe_3O_4) at about 300–350 ºC and magnetite to metallic iron at about 600–650 ºC.

In the same way, only two peaks of mass loss associated with the gradual reduction of hematite can be observed in Fig. 4b, since the first peak at temperatures below 200ºC would correspond to degassing and moisture removal. As can be derived from Fig. 4b, the hematite reduction process under CO rich atmospheres consists of two steps [51]: hematite (Fe_2O_3) to magnetite (Fe_3O_4) at around 300 ºC and magnetite (Fe_3O_4) to metallic iron at about 550 ºC.

According to the TPR and thermogravimetry results, which indicated that the most suitable reduction temperature was between 300 – 400 ºC, a reduction temperature of 300 ºC was selected. At higher temperatures, the thermal migration of potassium from the solid electrolyte to the Fe catalyst surface would hinder the adsorption of H_2 (electron donor) and therefore the reduction of Fe_2O_3 to Fe_3O_4 [52]. Furthermore, according to the phase diagram for the reduction of iron oxides at different H_2

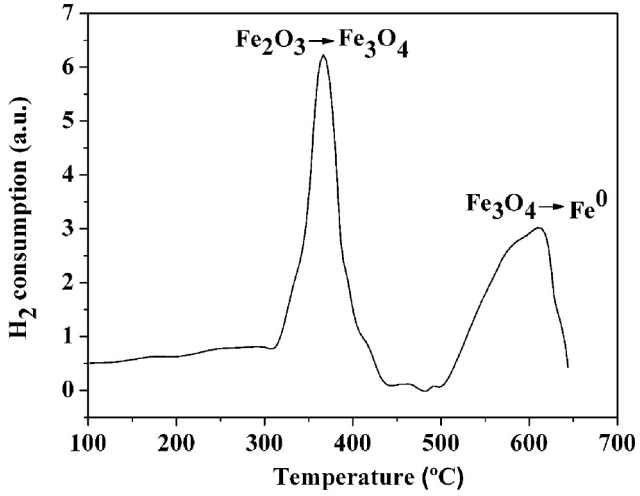

Fig. 3. TPR profile of the Fe_2O_3 powdered catalyst under 4% H_2 in He.

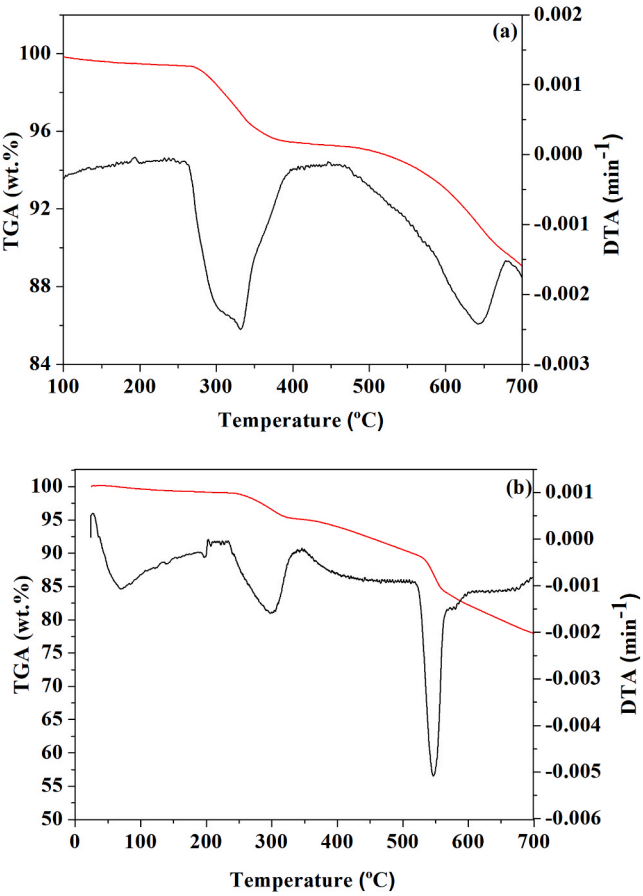

Fig. 4. TGA (red) and DTA (black) curves of the Fe_2O_3 powdered catalyst under (a) 4% H_2 in N_2 and (b) 5% CO in N_2.

concentrations and temperatures [49], it was decided to use a stream of 75% H_2 in He or N_2 as reducing gas, since the reduction in pure hydrogen would result in direct transformation of hematite to metallic iron, which favours carbon deposition. Nevertheless, before the last long-term electropromoted CO_2 hydrogenation test, the electrocatalyst was pre-reduced in pure H_2 at 400 °C for 8 hours, since according to the literature [49], these conditions favours the reduction of Fe_2O_3 to metallic iron that also promotes the formation of iron carbides (χ-Fe_5C_2) active for the Fischer-Tropsch reaction upon testing at 350 °C. However, it was visually observed that the Fe film had darkened significantly after the last long-term CO_2 hydrogenation test at 350 °C, which could be related to carbon deposition on the Fe surface. To confirm this fact, a SEM-EDX analysis of the aged Fe electrocatalyst was carried out once it was discharged from the reactor. A SEM image of the aged Fe film-solid electrolyte interface is shown in Fig. 5a, whereas an EDX mapping of Fe and C is shown in Figs. 5b and 5c, respectively. In addition, Fig. 6 presents a comparison between the surface aspect of different areas of the aged Fe film: a grey one (Fig. 6a), attributed to the presence of magnetite (Fe_3O_4) active phase, and a black one (Fig. 6b), attributed to carbon deposition.

As can be seen in Fig. 5, after exposure to reduction (at 400°C in pure H_2) and long-term testing (at 350 °C) conditions, carbon had been deposited over the Fe film, which may result in potential electrocatalyst deactivation by cooking or fooling.

It seems that, after exposure to reduction (at 400°C in pure H_2) and long-term testing (at 350 °C) conditions, the magnetite area of the Fe film resembled a spongy surface appearance, typical of a porous coating (allowing reactants and products diffusion) as can be observed in Fig. 6a. On the contrary, some agglomerates can be observed in the SEM image of the deposited carbon area (Fig. 6b), which are thought to be related with sintering of iron particles upon exposure to testing gas environment.

XRD patterns of the Fe film, both as prepared (after Fe deposition and calcination), after reduction (in 75% H_2 in N_2 at 300 °C) to form the magnetite active phase and after exposure to reduction (at 400°C in pure H_2) and long-term testing (at 350 °C) conditions are compared in Fig. 7.

The peaks at around 2θ=33°, 35.64° and 69.7° in the as prepared sample were identified as diffraction peaks of α-Fe_2O_3 (JCPDS card no. 01–073–0603), whereas in the samples after testing and/or reduction, the peaks at about 2θ=35.5° and 37° can be ascribed to Fe_3O_4 (JCPDS card no. 01–019–0629) and the peak at around 44.2° can be attributed to χ-Fe_5C_2 (JCPDS card no. 01–051–0997) or to carbon deposition (JCPDS card no. 01–080–0017).

Low intensity reflections of the Fe_2O_3 and Fe_3O_4 phases were observed in the XRD pattern of the as-deposited and as-reduced (in 75% H_2 in N_2 at 300 °C) sample, respectively. This seems to indicate that the as-deposited and as-reduced Fe film could be nanocrystalline.

In fact, the average crystallite size of the magnetite phase in the as-reduced (in 75% H_2 in N_2 at 300 °C) sample was estimated from X-ray broadening of the Fe_3O_4 diffraction peak at 2θ = 35.5 by using the well-known Debey-Scherrer equation [54], and resulted to be of about 22 nm, which, according to literature [55], is within the range of particle sizes considered to be appropriate, in terms of iron reducibility and availability of iron active sites, for effective CO_2 hydrogenation to C_{5+} hydrocarbons.

Reflections associated with χ-Fe_5C_2, resulting from carburization of Fe_3O_4 under exposure to the reaction environment, appear in the aged (after reduction at 400°C in pure H_2 and long-term testing at 350 °C) sample. The intensity of diffraction peaks associated with Fe_3O_4 and Fe_2O_3 considerably increases in the aged sample, indicating the formation of larger crystallites. This fact may be ascribed to re-oxidation of χ-Fe_5C_2 to Fe_3O_4 and of Fe_3O_4 to Fe_2O_3 by reaction with unconverted CO_2 or with H_2O generated by the CO_2 hydrogenation reaction, while Fe_2O_3 is reduced back to Fe_3O_4 in the presence of H_2 [50,56].

By comparison of the XRD patterns of grey (magnetite) and black (deposited carbon) areas in aged sample, it can be derived that, under the conditions of the last long-term test, the Fe film sintered giving rise to a decrease in particle size and a loss of crystallinity, as can be deduced from the decrease in the intensity of XRD peaks associated with Fe_2O_3, Fe_3O_4 and χ-Fe_5C_2.This may be the result of the oxidation-reduction cycles and transformations among different iron phases (Fe_2O_3, Fe_3O_4 and Fe_5C_2), which have been reported to take place during the RWGS and Fischer-Tropsch CO_2 hydrogenation processes [50].

The results of XPS analysis revealed the presence of various

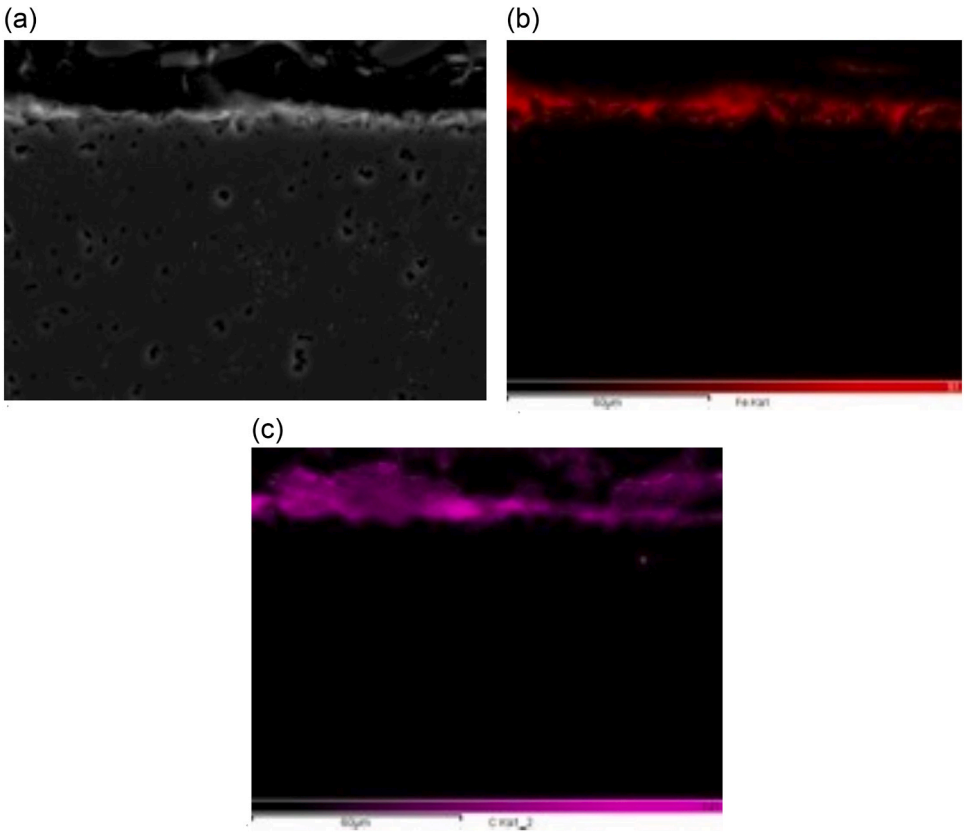

Fig. 5. SEM-EDX analysis of the aged (after reduction at 400ºC in pure H_2 and long-term testing at 350 ºC) Fe film-solid electrolyte interface: SEM image (a) and Fe (b) and C (c) distribution.

superficial iron compounds, resulting in Fe being present mainly as Fe_2O_3 in the as prepared sample, as shown by the appearance of peaks at binding energies of about 710.6 and 712.1 eV in the Fe 2p3/2 spectra (Fig. 8a) and at a binding energy of about 55.4 eV in the Fe 3p spectra (Fig. 8b). The appearance of a peak at 532 eV in the O1s spectra (Fig. 8c) seems to confirm the presence of Fe_2O_3 in the as prepared sample.

It seems that the pre-reduction (in 75% H_2 in N_2 at 300 ºC) of the Fe catalyst film, gave rise to an almost complete reduction of Fe_2O_3 to Fe_3O_4, as seems to indicate the presence of peaks at binding energies of about 709.2 and 711.1 eV in the Fe 2p3/2 spectra (Fig. 9a) and at about 530.3 eV in the O1s spectra (Fig. 9b).

3.2. CO_2 hydrogenation tests

3.2.1. Initial screening tests

Firstly, screening tests were carried out to study the influence of operating conditions on the CO_2 hydrogenation process. However, pairing the RWGS reaction (endothermic) with the Fischer-Tropsch reaction (exothermic) is not straightforward, given that the former is favoured at high temperatures and the later at low temperatures (around 200–350 ºC). CO_2 adsorption and dissociation to CO, i.e. the RWGS reaction, is considered the initial limiting step in the CO_2 hydrogenation to hydrocarbons [57], thus the effect of temperature, applied potential and gas flowrate on the RWGS process is analysed in this section.

a) Effect of temperature

Firstly, experiments were performed in order to identify a suitable operating temperature for the CO_2 hydrogenation process under unpromoted conditions, i.e., over a potassium-clean Fe surface. The tests were carried out varying temperature from 200 to 400 ºC upon application of 3 V, at 1500 NmL min^{-1}, under atmospheric pressure and using a H_2/CO_2 ratio of 3. The main products obtained were CO and CH_4.

Fig. 10a shows the effect of temperature on the conversion of CO_2 and on the selectivity to CO and CH_4 whereas Fig. 10b shows the variation in the rates of CO_2 conversion and CO and CH_4 formation with temperature.

As can be observed in Fig. 10a, over an electrochemically cleaned Fe surface (3 V), CO was preferentially formed over CH_4 under the studied operating conditions. CH_4 selectivity increased with temperature reaching a maximum at about 225 ºC, whereas CO selectivity monotonically increased with temperature, given that, at higher temperatures, reverse water gas shift (endothermic) (2) and methanation (exothermic) (4) reaction is thermodynamically favoured and retarded [58], respectively. CO_2 conversion increases with temperature especially at temperatures above 350 ºC where the RWGS reaction (endothermic) is favoured.

According to catalyst characterization results, initially deposited iron oxides (mainly as α-Fe_2O_3) were transformed into Fe_3O_4 (active phase for RWGS) during pre-reduction in 75% H_2 flow at 300 ° C.

It has been reported [57,59,60] that at low temperatures, formation of CO and reactive surface carbon species take place on the catalyst surface. The hydrogenation of reactive surface carbon species results in methane formation [57], which reached a maximum at 225 ºC, and then decreased with temperature increment. On increasing temperature, CO yield increases via the RWGS reaction which is a reversible endothermic reaction.

As can be observed in Fig. 10a, selectivity to CO and CH_4 seem to stabilize at temperatures above 300 ºC. However, the conversion of CO resulting from RWGS into hydrocarbons via Fischer-Tropsch synthesis reaction, which takes place on the iron carbide active phase of the multifunctional catalyst, is favoured at temperatures below 350 ºC. Therefore, a temperature value of 300 °C was selected for the subsequent potenciostatic tests.

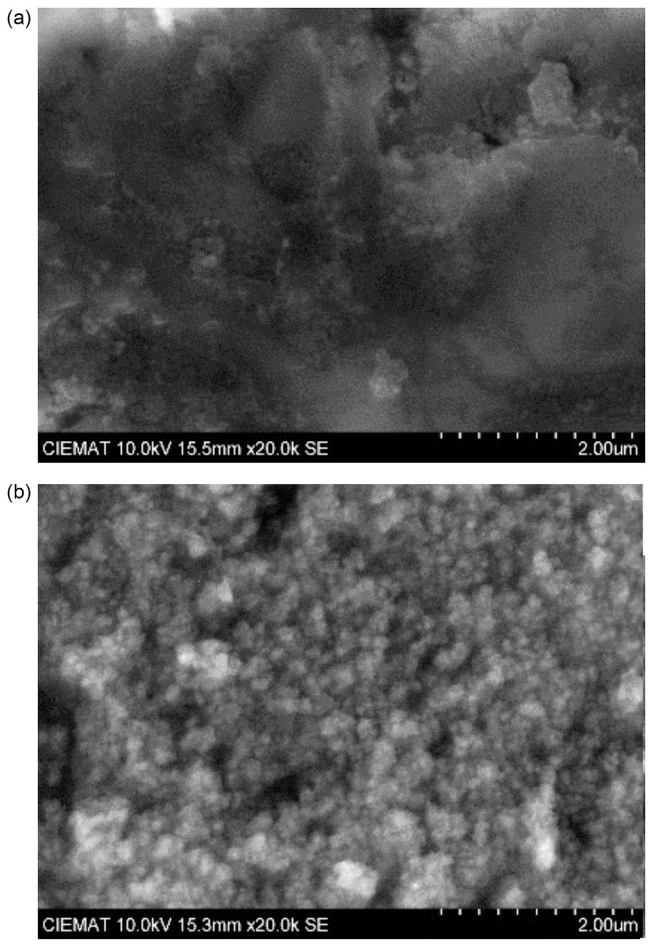

Fig. 6. SEM images of the aged (after reduction at 400 °C in pure H_2 and long-term testing at 350 °C) Fe film surface: (a) grey area (Fe_3O_4) and (b) black area (deposited carbon).

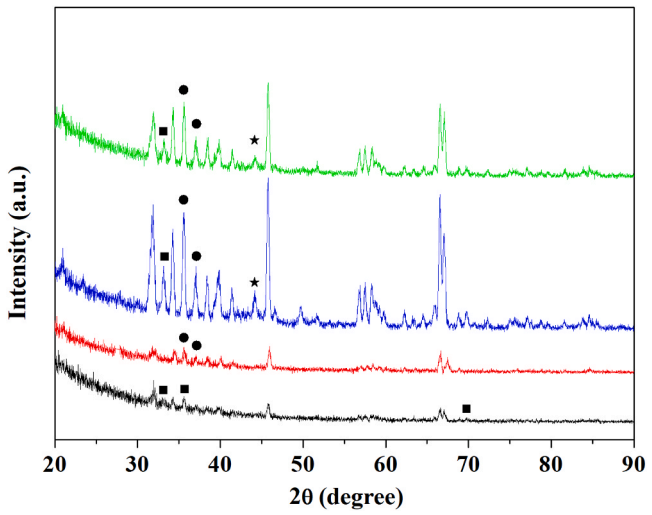

Fig. 7. XRD analysis of the Fe catalyst-electrode film: (a) as prepared (black), (b) after reduction at 300 °C in 75% H_2 in N_2 (red) and after reduction at 400 °C in pure H_2 and long-term testing at 350 °C: grey area (blue) and black area (green). Fe_2O_3 (■), Fe_3O_4 (●) and Fe_5C_2 (★).

On the other hand, as can be deduced from Fig. 10b, the magnetite formed during the pre-reduction step resulted to be active for the RWGS reaction, since the variation of CO_2 conversion rate with temperature practically coincides with that of CO formation rate.

b) Effect of potential

Fig. 11 depicts the effect of decreasing applied potential from 3 to −2.5 V on the electrochemically promoted CO_2 hydrogenation. The experiments were carried out at 1 bar, 300 °C and 1500 NmL min^{-1} and using a H_2/CO_2 ratio of 3. The accumulated amount of potassium promoter transferred to the catalyst surface estimated for each applied potential is also depicted in Fig. 11. According to the Faraday law, only negative values of current (potassium supplied to the catalyst surface) has been considered in Fig. 11, because positive values of current only represent the transfer of potassium ions back to the solid electrolyte from the catalyst surface.

As can be observed in Fig. 11a, under the utilized operating conditions, the hydrogenation of CO_2 over Fe/K-β-Al_2O_3 results mainly in the formation of CO and CH_4. Selectivity to CO is high whereas CO_2 conversion and selectivity to CH_4 are rather low. CO selectivity increased while CH_4 selectivity decreased, with opposite trends, as the applied potential decreased, i.e. RWGS reaction is favoured over methanation reaction on decreasing applied potential. Therefore, the selectivity to CO can be maximized by optimization of the applied potential, i.e. of potassium doping of Fe, reaching values of up to 99.5% at −2 V.

As can be also observed in Fig. 11a, CO_2 conversion and selectivity to CO (RWGS) increases with decreasing applied potential, i.e. with the presence of the electrochemical promoter (K^+) on the Fe catalyst surface, showing an electrophilic electrochemical behaviour [23], reaching a maximum at about −2 V, where both start to drop. Although applied negative potentials enhance chemisorption of electron acceptor molecules (CO_2), excessive pumping of K^+ to the Fe catalyst surface can also inhibit CO_2 adsorption, which may explain the decrease in CO selectivity and CO_2 conversion. On the contrary, selectivity to CH_4 diminishes with potential decrease, i.e. methanation reaction exhibits an electrophobic electrochemical behaviour [23].

The observed electrocatalytic behaviour can be explained by considering the effect of the transfer of potassium promoter ions from the solid electrolyte to the Fe catalyst surface (and vice versa), on the chemisorptive bond strength of reactants and intermediate species over the electrocatalyst surface, as well as based on the reaction mechanisms proposed for the CO_2 hydrogenation [35,37,38].

Decreasing applied potential to negative values results in the migration of potassium promoter species from the solid electrolyte to the Fe catalyst electrode, giving rise to a decrease of the catalyst work function, i.e., the electrode becomes negatively charged (due to an excess of electrons), which favours the transfer of electrons from the Fe catalyst to electron acceptor molecules (CO_2) and, thus, the adsorption of the latter on the Fe catalyst surface, whereas at the same time hindered the adsorption of electron donor species (H_2), giving rise to an increase in CO_2 (electron acceptor) coverage and to a decrease in the coverage of H_2 (electron donor).

The application of highly positive potentials gives rise to a migration of the electropositive

promoter (potassium ions) back to the solid electrolyte, resulting in an increase of the catalyst work function, i.e., the electrode becomes positively charged (due to a defect of electrons), which favours the transfer of electrons from electron donor molecules, like H_2, to the Fe catalyst and thus the adsorption of the latter on the Fe catalyst surface, whereas at the same time hindered the adsorption of electron acceptor species (CO_2), giving rise to an increase in H_2 (electron donor) coverage and to a decrease in the coverage of CO_2 (electron acceptor).

CO_2 can be chemisorbed (16) and at least partly dissociated to CO

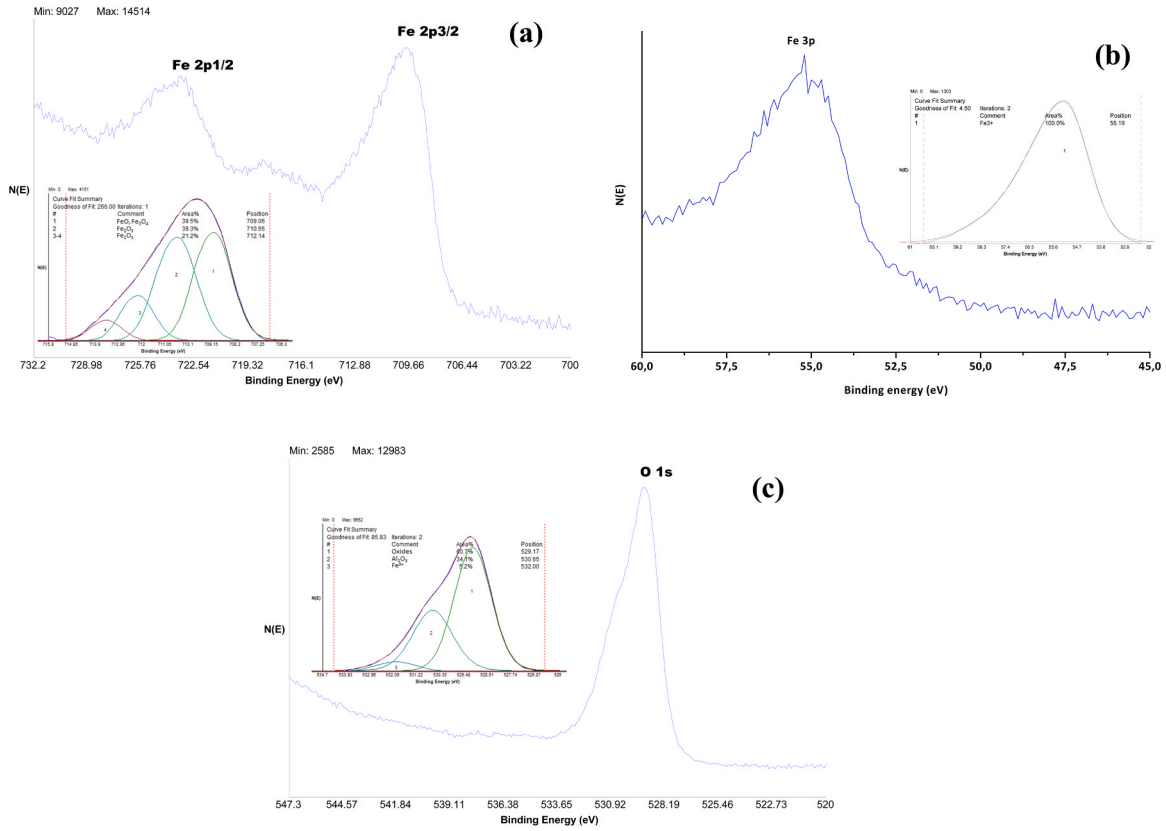

Fig. 8. XPS analysis of the Fe catalyst-electrode film as prepared: (a) Fe 2p3/2 XPS spectra, (b) Fe 3p XPS spectra, (c) O 1 s XPS spectra.

(17) over iron species (mainly Fe_3O_4) on a clean (at 3 V) Fe catalyst surface [61].

$$CO_2 + e^- \rightarrow CO_2^{*-}(ads.) \quad (16)$$

$$CO_2^{*-}(ads.) \rightarrow CO^*(ads.) + O^*(ads.) \quad (17)$$

The application of positive potentials favours the dissociative adsorption of hydrogen (electron donor) (18), so that the surface coverage of hydrogen increases and that of CO_2 (electron acceptor) decreases. Although, CO_2 dissociative adsorption can be also favoured in the presence of co-adsorbed hydrogen (19). The CO generated by the dissociative adsorption of CO_2 can be desorbed (RWGS reaction) (20), dissociated to surface carbon species that may accumulate on the catalyst surface (carbon deposition) (21) or gradually hydrogenated to hydrocarbons (CH_4) (22).

$$H_2 \rightarrow 2\,H^{*+}(ads.) + 2e^- \quad (18)$$

$$CO_2^{*-}(ads.) + e^- + 2H^{*+}(ads.) \rightarrow CO^*(ads.) + H_2O \quad (19)$$

$$CO^*(ads.) \rightarrow CO \quad (20)$$

$$CO^*(ads.) + e^- \rightarrow C^*(ads.) + O \quad (21)$$

$$C^*(ads.)\ (CH_4\ precursors) + O(ads.) + 6\,\mathrm{H}(ads.) \rightarrow CH_4 + H_2O \quad (22)$$

In general, according to the rules of electrochemical promotion, at high positive potentials, the surface coverage of hydrogen is higher than that of the species resulting from CO_2 or CO dissociation. This favours the formation of hydrocarbons (CH_4) and the desorption of CO (a weaker electron donor than H_2) so that the RWGS reaction is also favoured.

The increase in the amount of potassium transferred to the electrocatalyst surface on decreasing applied potential, promotes CO_2 (electron acceptor) dissociative adsorption to CO (16−17), due to a strengthening of Fe-(CO_2)* and Fe-C bonds and a weakening of C-O bond. On the contrary, dissociative adsorption of H_2 (electron donor) and CO (less electronegative than CO_2) are hindered. This entails a lower selectivity towards hydrocarbons (CH_4), since H_2 tend to be evolved from the catalyst surface (23), and thus, hydrogen coverage would be lower than that required for the carbon surface species to be completely hydrogenated, which implies a greater selectivity towards CO and potential carbon accumulation on the catalyst surface.

$$2\,H^{*+}(ads.) + 2e^- \rightarrow H_2 \quad (23)$$

Therefore, it can be stated that the catalytic activity for CO_2 hydrogenation and the selectivity to the desired products can be controlled by modifying the applied potential.

In addition, as can be observed in Fig. 11b, under applied potentials between −1.25 V and −2.5 V, the rates of CO_2 disappearance and CO formation practically coincide. Out of this range, a slight difference can be appreciated, indicating that the methanation reaction also contributes to CO_2 consumption. Therefore, it can be stated that, for applied potentials between −1.25 V and −2.5 V, magnetite is selective for the CO formation reaction (RWGS). These results suggest that the potential where the RWGS reaction would be more favoured over methanation is −2 V.

As can be observed in Fig. 11c, under application of −2 V, ρCO reached a maximum value (about four) while ρCH_4 reached a minimum value. This could be due to the fact that on decreasing the applied potential, the dissociative adsorption of CO_2 and CO is favoured and that of H_2 is hindered. Therefore, the formation of CO and surface carbon species increases at the expense of hydrocarbon (CH_4) formation. On the other hand, the decrease in applied potential led to

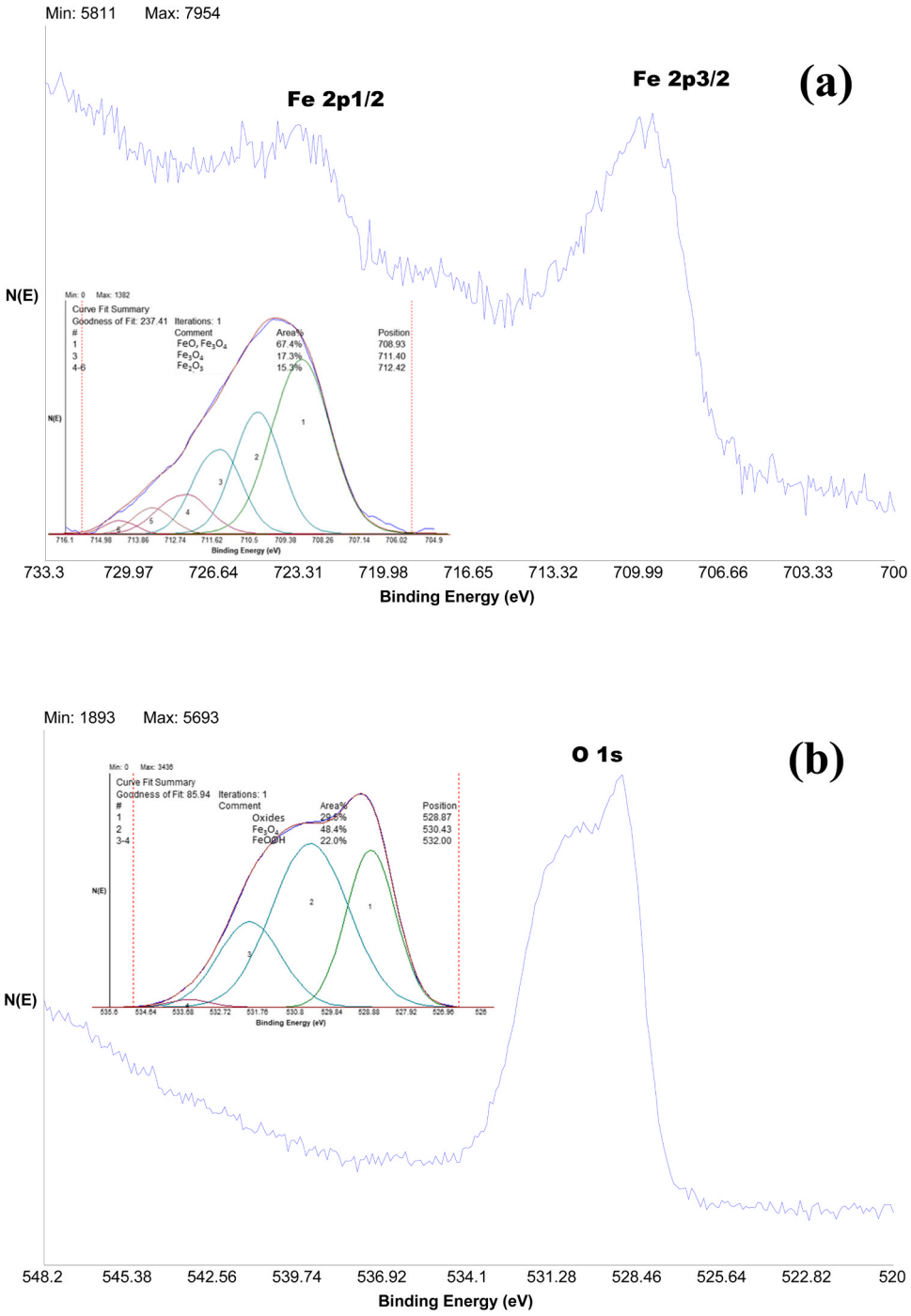

Fig. 9. XPS analysis of the Fe catalyst-electrode film after reduction at 300 ºC in 75% H_2 in N_2: (a) Fe 2p3/2 XPS spectra, (b) O 1 s XPS spectra.

a progressive decrease in the surface coverage of hydrogen, so that there was not enough hydrogen to remove the surface carbon species which, at potentials below −2 V, tend to accumulate on the catalyst surface giving rise to a decrease in the value of ρ_{CO} and of Λ_{CO} caused by a possible partial blockage of the electrocatalyst-solid electrolyte interface, which hinders the migration of K^+ to the catalyst surface [35,38]. Values of $\rho > 1$ is a distinctive attribute of electrochemical promotion vs. electrocatalysis [23], i.e., the higher the ρ value, the most pronounced the NEMCA effect.

As can be observed in Fig. 11d, $|\Lambda|_{CO} > 1$ at applied potentials below 2 V, the highest values of $|\Lambda|_{CO}$ can be appreciated at 1.5 and −2 V and resulted to be 9.9 and 4.4, respectively. Values of $|\Lambda| > 1$ is a differentiating attribute of electrochemical promotion vs. electrocatalysis [23]. In addition, the higher $|\Lambda|$, the strongest the NEMCA effect. According to these results, 1.5 V is the optimal potential for CO formation via RWGS reaction. In spite of $|\Lambda|_{CH4}$ values remain below 1 for any applied potential, it also shows a maximum at 1.5 V.

Based on these results, two long-term operating scenarios were explored: the first at 1.5 V to provide higher surface coverage of H_2 as to promote CO_2/CO hydrogenation to hydrocarbons. The latter at −2 V to enhance CO_2 dissociative adsorption and CO yield, via the RWGS reaction, which could subsequently be converted into hydrocarbons by the Fischer-Tropsch reaction over the Fe carbide active phase, the formation of which is also enhanced in the presence of high CO concentrations and potassium surface coverage [16,17].

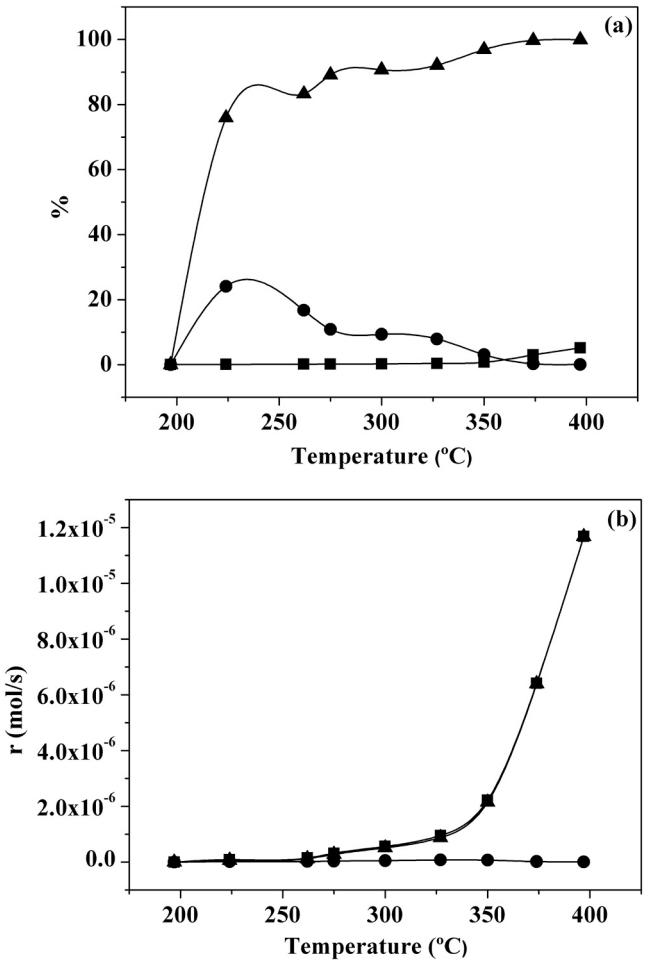

Fig. 10. Influence of temperature on (a) (■) CO_2 conversion and on selectivity to (●) CH_4 and (▲) CO and (b) rates of (■) CO_2 conversion and (●) CH_4 and (▲) CO formation. (1 bar, 1500 NmL min^{-1}, $H_2/CO_2 = 3$, 3 V).

c) Effect of gas flowrate

In order to analyse the impact of gas flowrate variation on the catalyst performance towards CO_2 hydrogenation, an additional series of tests was carried out under unpromoted conditions (at 3 V), at the temperature selected from previous tests (300ºC) and using a H_2/CO_2 ratio of 3. Fig. 12 shows the effect of gas flowrate variation (between 150 and 1500 NmL min^{-1}) on CO_2 conversion (Fig. 12a) and on the selectivity to CO and CH_4 (Fig. 12b).

Results on Fig. 12 indicate that increasing gas flowrate, and correspondingly, decreasing gas residence time in the reactor, resulted in a decrease in CO_2 conversion and CH_4 selectivity, whereas CO selectivity increases. These results seem to indicate that RWGS (CO formation) and methanation reactions are competitive and occur simultaneously. Therefore, it can be concluded that the increase in gas flowrate favours RWGS reaction at the expenses of CO_2 methanation. These results also confirm that under the previous utilized operating conditions (at 1500 NmL min^{-1}), the system was free from mass transfer limitations, given that CO_2 conversion diminished on increasing gas flowrate up to about 1250 NmL min^{-1}, from where it remains almost constant with gas flowrate increment.

According to these results, a gas flowrate of 300 NmL min^{-1}, from which CO selectivity remains almost constant with the variation of gas flowrate while CO_2 conversion is still high enough, was selected for the long-term catalyst performance tests. This will make it easier to appreciate the variations in CO_2 conversion and selectivity to the different products derived from possible catalyst activation or deactivation phenomena during the long-term tests.

3.2.2. *Long-term CO_2 hydrogenation tests*

As reported in literature [56] active species for RWGS are generally obtained by the reduction of α-Fe_2O_3 to Fe_3O_4. Moreover, during CO_2 hydrogenation, Fe_3O_4 phase is reported to disappear slowly and a new phase (χ-Fe_5C_2) is formed, which appears to be active for the Fischer-Tropsch reaction.

According also to literature [61] CO_2 can be at least partially dissociated to CO on the Fe_3O_4 species and in part decomposed further to carbon (24), which may result in catalyst deactivation by deposition of carbonaceous material and in Fe carburization to form the active phase (χ-Fe_5C_2) for the Fischer-Tropsch reaction. Simultaneously, χ-Fe_5C_2 can be re-oxidized to Fe_3O_4 (inactive for Fischer-Tropsch reaction and active for RWGS) by the oxygen released by CO_2 and CO dissociation. Moreover, Fe_3O_4 may capture surface oxygen and converts itself into Fe_2O_3 (inactive for RWGS and carbon deposition), which may also result in catalyst deactivation.

$$CO_2^{*-}(ads.) \rightarrow C^*(ads.) + 2\,O^*(ads.) \quad (24)$$

CO_2 hydrogenation over Fe based conventional catalyst (unpromoted conditions) is reported to proceed [56,59] via a two-step process, with initial reduction of CO_2 to CO via RWGS reaction over Fe_3O_4 and subsequent C-C chain growth over χ-Fe_5C_2 to form hydrocarbons via Fischer-Tropsch reaction. Moreover, iron oxides are also reported to be active to form oxygenates from CO [62].

According to literature [59,61,63], the mechanism of CO_2 hydrogenation on Fe based catalyst implies firstly CO_2 dissociative adsorption to adsorbed CO (16) on the catalyst surface. CO adsorbed species resulting from CO_2 dissociation may desorb in the gas phase (19 or 20) or can react with H_2 to form CH_3OH (25) and C_2H_6O (26). In addition, according to previous studies on electrochemical promotion of the Fischer-Tropsch synthesis reaction (3) by potassium [18,19] on Rh or by sodium on Ru [34], adsorbed CO can also dissociate to form surface carbon species (21), which can be hydrogenated to form CH_2 adsorbed species (27). Subsequent hydrogenation of CH_2 species gives rise to adsorbed CH_3 species (28) which can be further hydrogenated to CH_4 (29) or can react with adsorbed CO to form CH_3CO adsorbed species (30) which subsequent hydrogenation results in ethanol formation (31) [63]. Both CH_2 and CH_3 species are regarded as carbon-carbon propagation species with chain growth taking place, presumably, by successive addition of CH_2 units (33) to a growing alkyl radical (32) resulting in the formation of alkanes or alkenes by hydrogenation (34) or β-hydrogen elimination (35) of the growing alkyl radical, respectively.

$$CO^*(ads.) + 4\,H^*(ads.) \rightarrow CH_3OH \quad (25)$$

$$3\,CO^*(ads.) + 6\,H^*(ads.) \rightarrow CH_3OCH_3 + CO_2 \quad (26)$$

$$C^*(ads.) + 4\,H^*(ads.) \rightarrow CH_2^*(ads.) \quad (27)$$

$$CH_2^*(ads.) + H^*(ads.) \rightarrow CH_3^*(ads.) \quad (28)$$

$$CH_3^*(ads.) + H^*(ads.) \rightarrow CH_4 \quad (29)$$

$$CH_2^*(ads.) + CO^*(ads.) + H^*(ads.) \rightarrow CH_3CO^*(ads.) \quad (30)$$

$$CH_3CO^*(ads.) + 3\,H^*(ads.) \rightarrow C_2H_5OH \quad (31)$$

$$CH_2^*(ads.) + CH_3^*(ads.) \rightarrow CH_3CH_2{}^*(ads.) \quad (32)$$

$$CH_3CH_2{}^*(ads.) + (n-2)\,CH_2^*(ads.) \rightarrow CH_3 - (CH_2)_{n-1}^*(ads.) \quad (33)$$

$$CH_3 - (CH_2)_{n-1}^*(ads.) + H^*(ads.) \rightarrow C_nH_{2n+2} \quad (34)$$

$$CH_3 - (CH_2)_{n-1}^*(ads.) \rightarrow C_nH_{2n} + 1/2\,H_2 \quad (35)$$

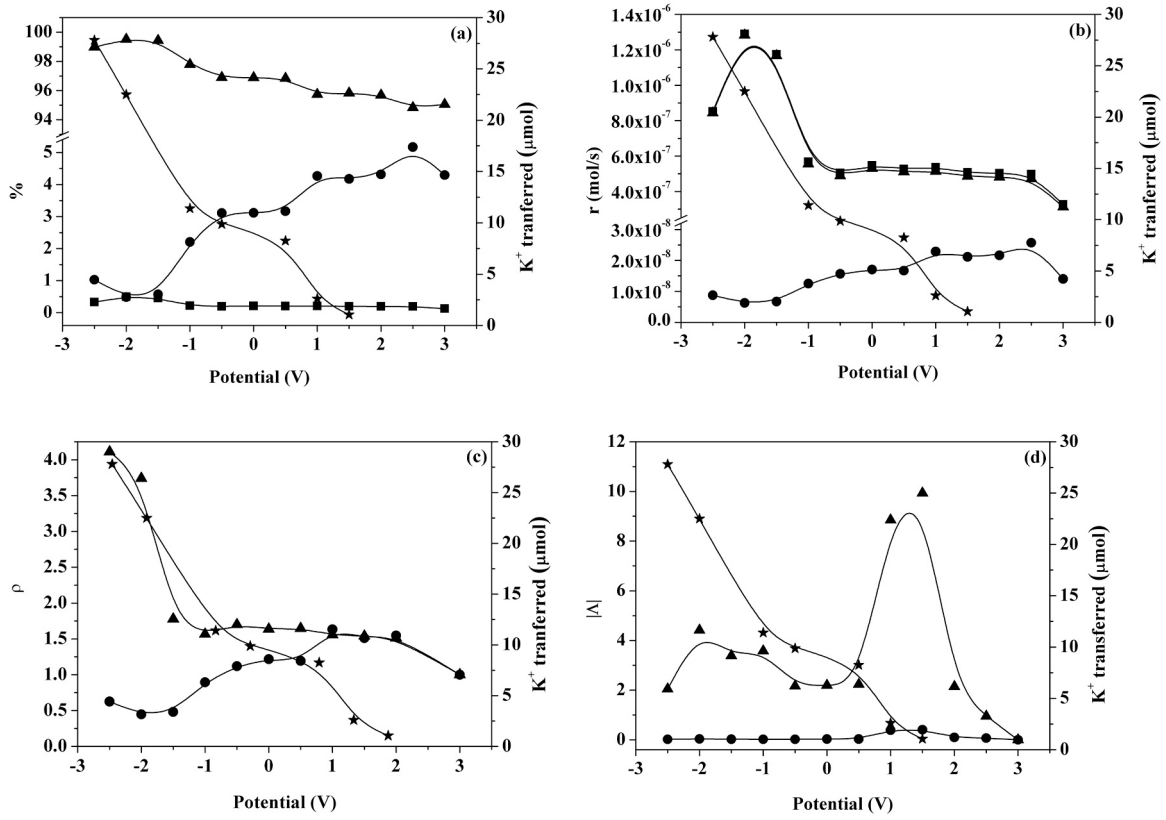

Fig. 11. Influence of applied potential on (a) (■) CO_2 conversion and selectivity to (●) CH_4 and (▲) CO, (b) rate of (■) CO_2 conversion and (●) CH_4 and (▲) CO formation, (c) rate enhancement ratio (ρ) of (●) CH_4 and (▲) CO and (d) apparent faradaic efficiency or NEMCA factor (Λ) of (●) CH_4 and (▲) CO. (1 bar, 1500 NmL min^{-1}, $H_2/CO_2 = 3$, 300 °C). (★) Potassium transferred to the catalyst surface upon potential application (μmol).

According to literature [64,65], the addition of potassium to the catalyst surface enhances Fe–C bonds and weakens C═O bonds, promoting CO_2/CO dissociation and facilitating CO_2 conversion, formation of iron carbides (active phase for C-C coupling) and carbon chain growth. However, there is an optimum in potassium loading. The addition of small amounts of potassium enhances CO_2 adsorption while inhibiting H_2 adsorption on the catalyst surface, resulting in a high carbon to hydrogen ratio which favours C–C coupling and hinders methane and methanol formation, leading to an increase in carbon chain length and branching, and therefore, in the selectivity to C_{5+} hydrocarbon fuels. On the contrary, adding potassium in excess may result in blocking of active sites by potassium and/or carbon deposition with the subsequent decrease in catalyst activity, selectivity and stability [64,65].

a) Electrochemically promoted CO_2 hydrogenation on Fe/K-β-Al_2O_3/Au

The variation of CO_2 conversion and selectivity to CO and C_{5+} hydrocarbons versus time on stream, upon application of a constant potential of 1.5 V during 48 hours and of −2 V for 24 hours at 300 °C, is shown in Figs. 13a and 13b, respectively. CH_4 and C_2-C_3 hydrocarbons (not shown) were also detected to be formed but in a very small quantity.

Results on Fig. 13 suggest that at early stages of the long-term tests, where selectivity to C_{5+} is higher, a partial carburization of the magnetite occurs. In this way, the CO resulting from RWGS on Fe_3O_4 can be converted to hydrocarbons, via the Fischer-Tropsch synthesis, on the previously formed iron carbide (χ-Fe_5C_2). It seems that, as reported in literature [56], at the first stages of the reaction, Fischer-Tropsch activity develops and is progressively stablished on the catalyst surface by slow transformation of Fe_3O_4 to χ-Fe_5C_2 via reaction between Fe and surface adsorbed carbon.

The electrochemical pumping of potassium to the Fe catalyst surface enhances Fe–C bonds and weakens C═O bonds, promoting CO_2/CO (electron acceptor) dissociative adsorption, increasing carbon and oxygen surface coverage, and formation of surface iron carbides (active for C-C coupling), by reaction between Fe and adsorbed surface carbon, while inhibiting H_2 (electron donor) dissociative adsorption, decreasing hydrogen coverage. This results in a high C/H ratio which favours C–C coupling and hinders methane and methanol formation by inhibition of the termination hydrogenation reactions, leading to an increase in carbon chain length, and therefore in the selectivity to C_{5+}, on increasing alkali loading [18,19]. After that, the selectivity to C_{5+} hydrocarbons decreases while the selectivity to CO (less electron acceptor than CO_2) increases up to a maximum as the alkali loading is increased, which seems to indicate that, χ-Fe_5C_2 was progressively re-oxidized to Fe_3O_4 (inactive for Fischer-Tropsch reaction and active for RWGS) by reaction with the oxygen released by CO_2/CO dissociation [56]. After a certain period of time, selectivity to CO decreased at the same time as that of C_{5+} increased, while CO_2 conversion hardly changed. This seems to indicate that, on increasing potassium coverage in the presence of relatively high CO concentrations, hydrocarbon synthesis becomes evident again. Subsequently, the selectivity to CO increased and that of C_{5+} decreased over time since the RWGS reaction once again turned dominant.

According to catalyst characterization results, initially deposited iron oxides (mainly as α-Fe_2O_3) were transformed into Fe_3O_4 (active phase for RWGS) during pre-reduction steps and partially to χ-Fe_5C_2 (active phase for Fischer-Trospch synthesis) during the long-term CO_2 hydrogenation tests. The catalyst characterisation results also point out at oxidation of χ-Fe_5C_2 to Fe_3O_4, re-oxidation of Fe_3O_4 to Fe_2O_3 and reduction of Fe_2O_3 to Fe_3O_4 taking place upon exposure to reaction gas environment and conditions.

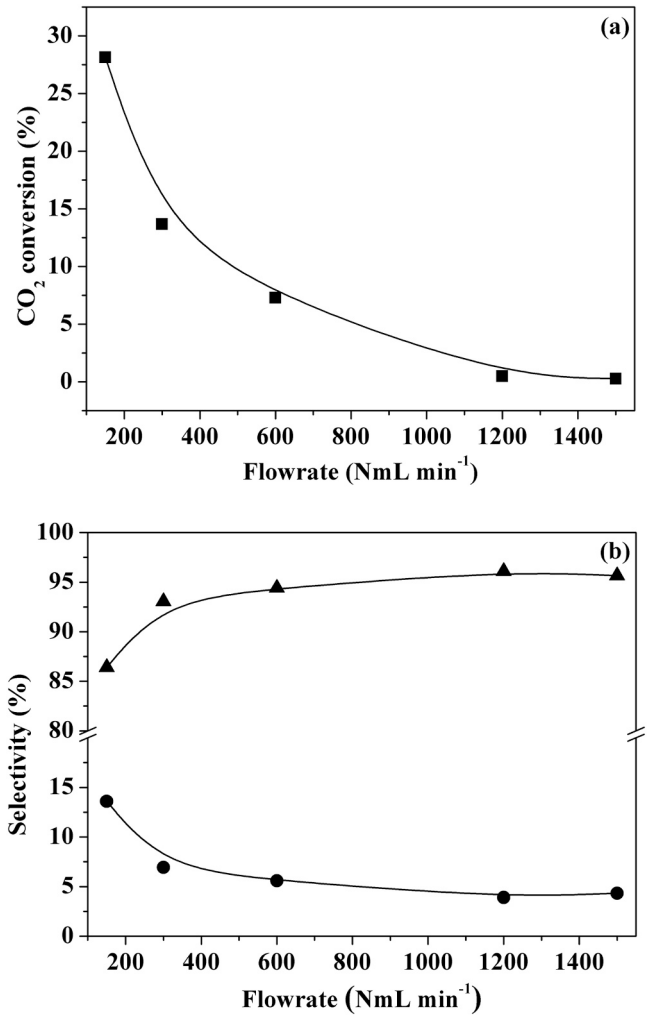

Fig. 12. Influence of gas flowrate on (a) CO_2 conversion (■) and (b) selectivity to (●) CH_4 and (▲) CO over the Fe film. (1 bar, 3 V, $H_2/CO_2 = 3$, 300 °C).

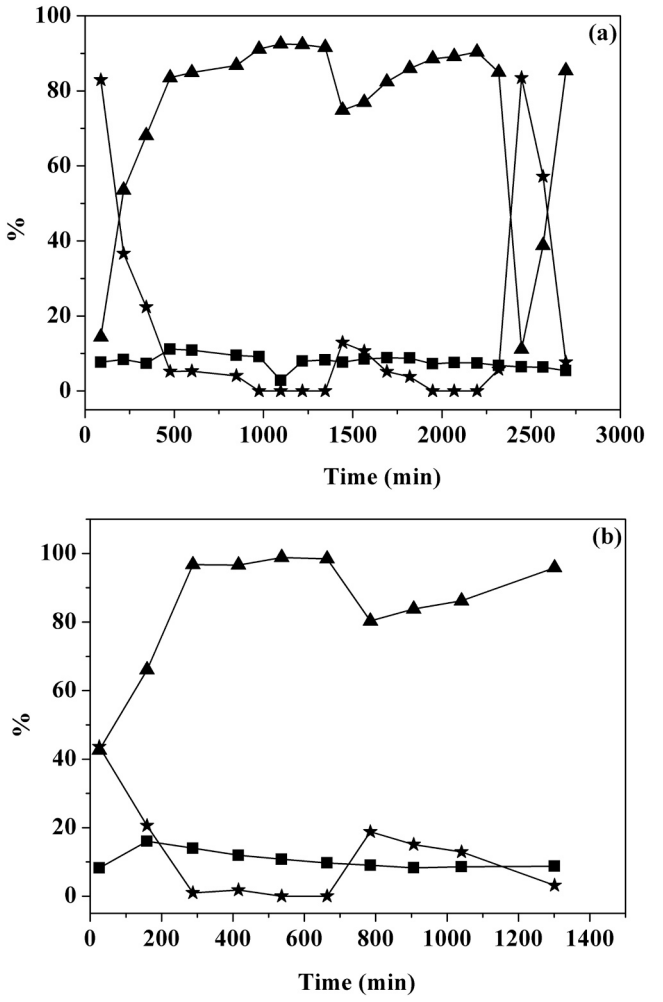

Fig. 13. Variation of (■) CO_2 conversion and selectivity to (★) C_{5+} hydrocarbons and (▲) CO with time on stream at (a) 1.5 V and (b) −2 V. (Pre-reduction in 75% H_2 in N_2 at 300 °C, 1 bar, 300 NmL min^{-1}, $H_2/CO_2 = 3$, 300 °C).

Therefore, the observed cyclic catalytic performance seems to indicate that the surface composition of the catalyst (iron oxides/carbides) changes with time on stream depending on the balance between the reactions that lead to the formation (RWGS) and consumption (synthesis of hydrocarbons and carbon deposition) of CO and oxidation/reduction/carburization of Fe [50], as seem to be confirmed also by catalyst characterisation results.

Almost no light hydrocarbon (C_1-C_4) formation was observed in these tests which seems to confirm that potassium favours the growth of hydrocarbon chains [64,65]. According to the above commented mechanism of CO_2 hydrogenation on Fe based catalysts, carbon chain growth takes place by consecutive addition of CH_2 adsorbed species (33) to a growing alkyl radical (CH_3CH_2*) (32), whereas carbon chain termination occurs by hydrogenation (34) of the growing alkyl radical, resulting in the formation of hydrocarbons with different chain lengths. Therefore, the fact that almost no light hydrocarbon formation was observed seems to indicate that, under testing conditions, chain growth, and thus the formation of longer chain hydrocarbons, is favoured over chain termination, because the electrochemical pumping of small amounts of potassium to the Fe catalyst surface enhances CO_2 (electron acceptor) adsorption while inhibits H_2 (electron donor) adsorption, hindering light hydrocarbon formation, as hydrogen coverage is lower than that required for the growing alkyl radical to be completely hydrogenated, and rendering a high surface carbon to hydrogen ratio which enhances C–C

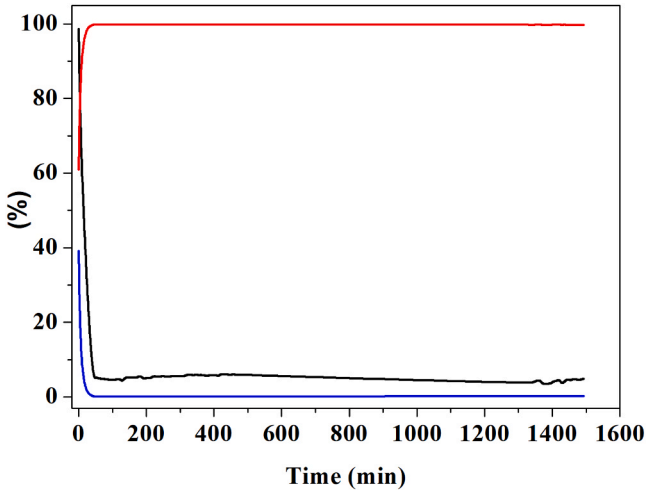

Fig. 14. Variation of CO_2 conversion (black) and selectivity to CO (red) and CH_4 (blue) with time on stream over the Fe film. (Pre-reduction in H_2 at 400 °C, 1 bar, 300 NmL min^{-1}, $H_2/CO_2 = 3$, 350 °C, 1.5 V).

coupling, leading to an increase in carbon chain length and branching, and therefore, in the selectivity to C_{5+} hydrocarbon fuels.

Finally, a long-term test was carried out under different pre-reduction, at 400 ºC for 8 hours in pure H_2, and CO_2 hydrogenation, at 350 ºC and +1.5 V for 24 hours, conditions. Fig. 14 shows the variation of CO_2 conversion and selectivity to CO and CH_4 vs. time on stream, under such conditions.

As commented in the above, according to the phase diagram for the reduction of iron oxides at different H_2 concentrations and temperatures [49], the Fe catalyst pre-reduction in pure hydrogen at 400 ºC may result in direct reduction of hematite to metallic iron, which promotes carbon deposition, but also the formation of iron carbides (χ-Fe_5C_2) active for the Fischer-Tropsch reaction. Moreover, according to literature [64,65], the addition of potassium to the catalyst surface enhances formation of iron carbides (active phase for C-C coupling) and carbon chain growth. However, there is an optimum in potassium loading. Operation of the Fe catalyst at higher temperatures (350 ºC) for the same applied potential (+1.5 V) may give rise to excessive potassium surface coverage, resulting in blocking of active sites by potassium and/or carbon deposition, due to the enhanced CO_2/CO dissociative adsorption and retarded hydrogen chemisorption on the catalyst surface as a result of the increased ionic conductivity of the solid electrolyte at higher temperatures, with the subsequent decrease in catalyst activity, selectivity and stability [64,65]. The formation of hydrocarbons other than CH_4 was practically negligible under the utilized pre-reduction and testing conditions. Furthermore, after testing, it was visually observed that carbon had been deposited on the Fe electrocatalyst film, as also confirmed by characterization results (SEM).

As can be observed in Fig. 14, at the beginning of the reaction CO_2 conversion and methane selectivity decreases rapidly whereas CO selectivity increases up to almost 100%. In addition, the high initial values of CH_4 selectivity are indicative that the Fischer-Tropsch regime was not stablished on the catalyst surface, whereas the sharp decrease in CO_2 conversion with increasing potassium doping over time suggests that Fe catalyst poisoning occur instead.

Carbon deposition and accumulation appears to have taken place during the initial stages of the reaction where the CO_2 conversion was highest, due to excessive CO_2/CO dissociation which is enhanced at the higher operation temperature utilized in this test, causing deactivation of the active sites for hydrocarbon (CH_4) synthesis.

It must be highlighted that the variation of selectivity to long chain hydrocarbons vs. time on stream, i.e., vs. potassium doping, is under a compromise between higher driving force in activity (iron carburization) and larger tendency to inert carbon deposition [59,66]. On the one hand, increasing temperature leads to a concomitant increase in the extent of carbon deposition and in the stability of the surface carbon species formed [66]. On the other hand, the ionic conductivity of the solid electrolyte, and thus the amount of potassium electrochemically pumped to the catalyst surface for the same applied potential, increases also with temperature. These effects result in an increase in CO selectivity and in suppressing selectivity towards hydrocarbons. This fact can be related with an excessive pumping of potassium to the catalyst surface which, on the one hand, may cover iron Fe active sites hindering CO_2 adsorption and its subsequent conversion, and, on the other hand, further strengthens Fe–C bond, hindering C desorption, and resulting in carbon deposition which progressively blocks the iron active sites [64,65]. In fact, as reported in literature [67], there is a potassium loading which maximizes Fischer-Tropsch activity. Potassium loadings above this value result in the formation of inert graphitic carbon, which may decrease the Fischer-Tropsch activity by carbon deposition on the catalyst surface.

It is generally accepted that the rate limiting step for the methanation reaction is carbon hydrogenation rather than CO_2/CO dissociation [68]. As potassium doping progressively increases over time, the dissociative adsorption of H_2 (electron donor) and CO (less electronegative than CO_2) are progressively hindered. Therefore, hydrogen coverage is increasingly less than that required for the carbon surface species to be completely hydrogenated, which leads to lower and higher selectivity to hydrocarbons (CH_4) and CO, respectively and potential carbon accumulation on the catalyst surface.

According to the stoichiometry of the reaction, methanation is more hydrogen demanding than the Fischer-Tropsch synthesis and thus methanation activity is more strongly suppressed by potassium addition to the catalyst surface, which may account for the faster decrease in selectivity to hydrocarbons (CH_4) observed in this test.

b) Conventional catalytic CO_2 hydrogenation on powdered catalysts

Long term tests on CO_2 hydrogenation over conventional Fe-KVO_3 powdered catalysts were also carried out with the aim of selecting the proper Fe loading for the reaction.

The results of the conventional catalytic CO_2 hydrogenation test over the Fe-KVO_3 catalyst with 17 wt% Fe are shown in Fig. 15. Fig. 15a depicts the variation of CO_2 conversion and selectivity to CO, CH_4 and C_{5+} hydrocarbons versus time on stream. Fig. 15b shows the variation of CO and CH_4 concentration at the reactor outlet with operating time.

As can be observed in Fig. 15, at the beginning of the test, CO_2 conversion was very high, but little CO and CH_4 were formed. This seems to confirm that an iron carbide phase (χ-Fe_5C_2), active for Fischer-Tropsch synthesis, may be formed by CO partial carburization of the magnetite resulting from pre-reduction of hematite. In addition,

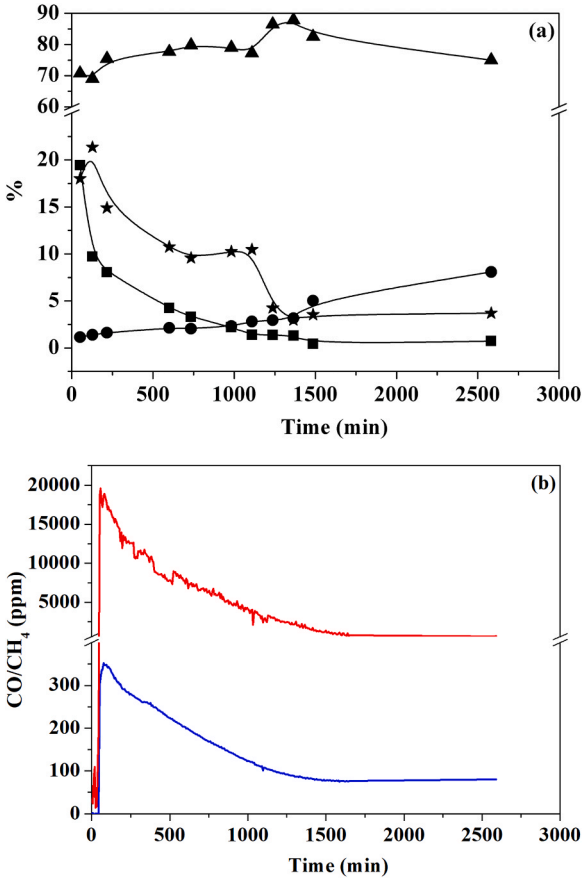

Fig. 15. Variation of (a) CO_2 conversion (■) and selectivity to C_{5+} hydrocarbons (★), CH_4 (●) and CO (▲) and (b) CH_4 (blue) and CO (red) content with time on stream over the Fe-KVO_3 (17 wt% Fe) catalyst. (13.5 bar, GHSV= 1400 h^{-1}, H_2/CO_2 = 3, 300 ºC).

selectivity to C_{5+} increased and that of CO decreased with increasing operation time up to a certain value which practically coincides with that corresponding to the maximum CO and CH_4 concentration in the exiting gas. This fact seems to confirm that the CO formed by RWGS on Fe_3O_4 is converted to C_{5+} hydrocarbons over χ-Fe_5C_2. After that, selectivity to C_{5+} hydrocarbons decreased while the selectivity to CO increased up to a maximum, supposedly due to re-oxidation of the iron carbide phase to magnetite by reaction with unconverted CO_2 or with the H_2O generated by the CO_2 hydrogenation reaction [56]. Then, selectivity to CO decreased and CH_4 selectivity increased, while CO_2 conversion and C_{5+} selectivity hardly varied. It seems that, during the second half of the test, the formation of CH_4 and light hydrocarbons (not shown) was increasingly favoured over that of long chain hydrocarbons (C_{5+}) with increasing time on stream, probably due to the smaller size of the utilized Fe nanoparticles, which favours the dissociative adsorption of CO_2 and CO on Fe to form carbonaceous compounds, which are considered reaction intermediates in the formation of methane, as well as the cracking of possible long-chain hydrocarbons, which may have been formed, to light hydrocarbons. However, the selectivity towards C_2 and C_3 hydrocarbons (not shown) resulted to be very low throughout the test due to the positive effect of potassium on the growth of hydrocarbon chains [64,65].

CO_2 conversion decreased also with increasing time on stream, supposedly due to deactivation by carbon deposition.

Therefore, Fe-KVO_3 (17% Fe) shows a similar cyclic catalytic performance than Fe/K-β-Al_2O_3/Au, but formation of CH_4 and light hydrocarbons was increasingly favoured over that of C_{5+} hydrocarbons and CO_2 conversion decreased with increasing time on stream, given the smaller size of the Fe nanoparticles which may favour CO_2/CO dissociative adsorption to carbonaceous compounds, resulting in deactivation by carbon deposition and methane formation, as well as long-chain hydrocarbons cracking.

The variation of CO_2 conversion and CO and CH_4 concentration at the reactor outlet vs time on stream for the Fe-KVO_3 catalyst with 9 wt% Fe are shown in Fig. 16.

As can be observed in Fig. 16, the formation of CO and CH_4 as main compounds derived from CO_2 hydrogenation was very low. Therefore, most of the initial CO_2 conversion can be attributed to the formation of carbon that rapidly deactivated the catalyst.

The Fe-KVO_3 (9 wt% Fe) catalyst deactivated very quickly, after about 4 hours, probably due to the higher K/Fe ratio of this catalyst which enhances carbon deposition [17,64,69] as a result of potassium overloading [44,45]. The Fe-KVO_3 (17 wt% Fe) catalyst was much more stable, but it also deactivated almost completely after about 25 hours due also to carbon deposition, as visually confirmed on both samples after testing. In addition, the catalyst with higher Fe loading, i.e., lower K/Fe ratio, shows much higher selectivity to long-chain hydrocarbon formation [17,64,69].

An additional conventional catalytic CO_2 hydrogenation study was performed over Fe_2O_3 powdered catalyst under the same operating conditions. The results are plotted in Fig. 17, which shows the variation of CO_2 conversion and selectivities to CO, CH_4 and C_2, C_3 and oxygenated hydrocarbons with time on stream.

As shown in Fig. 17, CO_2 conversion and CH_4 selectivity were maximum while CO selectivity was minimum at the beginning of the test. Furthermore, the opposite trend of CO and CH_4 selectivities versus time indicates that the RWGS and methanation reactions are competitive.

During the test, C_2, C_3 and oxygenates (such as methanol, ethanol, acetic acid or formic acid) hydrocarbons were formed. However, the selectivity towards C_{5+} hydrocarbons was practically zero, which may be due to the absence of potassium, which is reported [64,65] to promote the growth of hydrocarbon chains, in this catalyst.

Comparing the results obtained on the Fe-KVO_3 catalyst (17 wt% Fe) and those of the Fe_2O_3 catalyst, it can be assessed that, although the initial CO_2 conversion was slightly higher over the former, it decreased to practically zero, after approximately 25 hours of continuous operation, while the Fe_2O_3 catalyst still remain active, indicating that the latter is more stable, probably because the presence of potassium in the Fe-KVO_3 catalyst favours also carbon deposition.

Regarding the formation of hydrocarbons, it is observed that the Fe-KVO_3 (17 wt% Fe) catalyst exhibited higher selectivity to C_{5+}, whereas the hematite catalyst was more selective to C_2, C_3 and oxygenated hydrocarbons. This fact seems to be related to the presence of potassium in the Fe-KVO_3 catalyst which enhance the growth of hydrocarbon chains leading to a higher selectivity to C_{5+} hydrocarbons.

On the other hand, by comparison of the results of CO_2 hydrogenation on conventional Fe_2O_3 powdered catalyst and those over Fe/K-ß-Al_2O_3/Au electrocatalyst, it is confirmed that both selectivity to long chain hydrocarbons (C_{5+}) and carbon deposition can be controlled in situ by adjusting the surface coverage of the potassium, via electrochemical pumping of K^+ ions by modifying the applied potential, maximizing CO_2 conversion to the target product and increasing the useful life of the catalyst.

4. Conclusions

In this study, a Fe/K-β-Al_2O_3/Au tubular electrochemical catalyst has been successfully prepared by dip-coating and characterised, both as

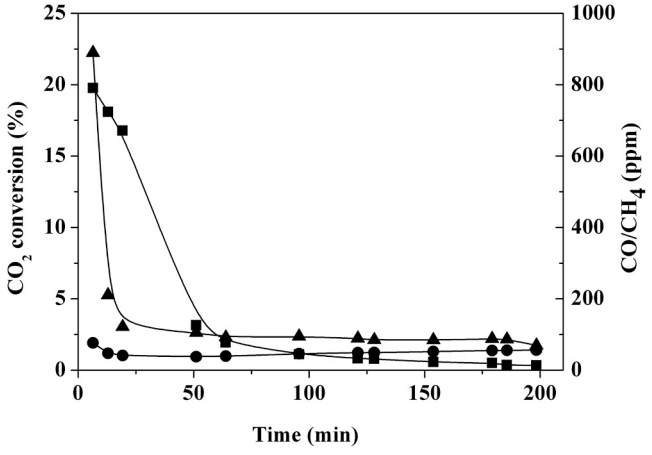

Fig. 16. Variation of (a) CO_2 conversion (■) and CH_4 (●) and CO (▲) outlet gas concentrations versus time on stream over the Fe-KVO_3 (9 wt% Fe) catalyst. (13.5 bar, GHSV= 1400 h^{-1}, H_2/CO_2 = 3, 300 °C).

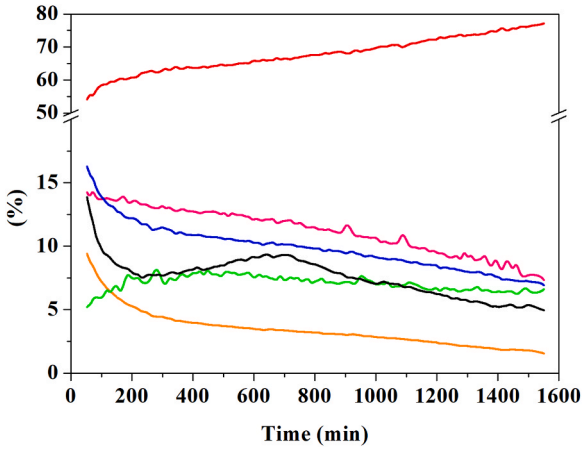

Fig. 17. Variation of CO_2 conversion (black) and selectivity to CH_4 (blue), CO (red) and C_2 (orange), C_3 (pink) and oxygenated (green) hydrocarbons versus time on stream over the Fe_2O_3 powdered catalyst. (13.5 bar, GHSV= 1400 h^{-1}, H_2/CO_2 = 3, 300 °C).

prepared and after reduction and testing under different operating conditions, by Scanning Electron Microscopy, X-Ray Photoelectron Spectroscopy and X-Ray Diffraction techniques.

The CO_2 hydrogenation to hydrocarbon fuels over Fe in a potassium ion conducting reactor can be electrochemically promoted under atmospheric pressure, at relatively low temperatures and using representative concentrated CO_2 and H_2 gas mixtures and easily scalable catalyst-electrode configurations, as an approach towards its potential practical application.

Selectivity to the target product (C_{5+} hydrocarbons) can be modulated by modifying applied potential under given operating conditions. The Fe/K-β-Al_2O_3 electrocatalyst was more active and stable when working at positive potentials (1.5 V), confirming that both the long-chain hydrocarbons (C_{5+}) yield and catalyst deactivation by carbon deposition can be tuned in-situ by modifying the surface coverage of potassium via electrochemical pumping of potassium ions by varying the applied potential.

The conventional Fe-KVO_3 catalyst with higher Fe loading (17 wt%) seems to be more promising, in terms of activity, selectivity and stability, for further electrocatalyst optimisation by deposition, via dip-coating, of a Fe-KVO_3 film on the K-β-Al_2O_3 candle.

Declaration of Competing Interest

The authors declare that they have no known competing financial interests or personal relationships that could have appeared to influence the work reported in this paper.

Data availability

The authors are unable or have chosen not to specify which data has been used.

Acknowledgements

This research did not receive any specific grant from funding agencies in the public, commercial, or not-for-profit sectors.

References

[1] G. Centi, S. Perathoner, Opportunities and prospects in the chemical recycling of carbon dioxide to fuels, Catal. Today 148 (2009) 191–205.
[2] F.D. Meylan, V. Moreau, S. Erkman, CO2 utilization in the perspective of industrial ecology, an overview, J. CO2 Util. 12 (2015) 101–108.
[3] Y. Jiang, K. Wang, Y. Wang, Z. Liu, X. Gao, J. Zhang, Q. Ma, S. Fan, T.-S. Zhao, M. Yao, Recent advances in thermocatalytic hydrogenation of carbon dioxide to light olefins and liquid fuels via modified Fischer-Tropsch pathway, J. CO2 Util. 67 (2023) 102321.
[4] J. Wei, R. Yao, Q. Ge, Z. Wen, X. Ji, C. Fang, J. Zhang, H. Xu, J. Sun, Catalytic hydrogenation of CO2 to isoparaffins over fe-based multifunctional catalysts, ACS Catal. 8 (2018) 9958–9967.
[5] M. Liu, Y. Yi, L. Wang, H. Guo, A. Bogaerts, Hydrogenation of carbon dioxide to value-added chemicals by heterogeneous catalysis and plasma catalysis, Catalysts 9 (2019) 275.
[6] W. Shafer, G. Jacobs, U. Graham, H. Hamdeh, B. Davis, Increased CO2 hydrogenation to liquid products using promoted iron catalysts, J. Catal. 369 (2018) 239–248.
[7] H. Yang, C. Zhang, P. Gao, H. Wang, X. Li, L. Zhong, W. Wei, Y. Sun, A review of the catalytic hydrogenation of carbon dioxide into value-added hydrocarbons, Catal. Sci. Technol. 7 (2017) 4580–4598.
[8] J. Ma, N. Sun, X. Zhang, N. Zhao, F. Xiao, Y. Sun, A short review of catalysis for CO2 conversion, Catal. Today 148 (2009) 221–231.
[9] R.-P. Ye, J. Ding, W. Gong, M.D. Argyle, Q. Zhong, Y. Wang, C.K. Russell, Z. Xu, A. G. Russell, Q. Li, M. Fan, Y.-G. Yao, CO2 hydrogenation to high-value products via heterogeneous catalysis, Nat. Commun. 10 (2019) 5698.
[10] J. Wei, Q. Ge, R. Yao, Z. Wen, C. Fang, L. Guo, H. Xu, J. Sun, Directly converting CO2 into a gasoline fuel, Nat. Commun. 8 (2017) 15174.
[11] J. Wei, R. Yao, Q. Ge, Z. Wen, X. Ji, C. Fang, J. Zhang, H. Xu, J. Sun, Catalytic Hydrogenation of CO2 to Isoparaffins over Fe-Based Multifunctional Catalysts, ACS Catal. 8 (2018).
[12] Y.H. Choi, Y.J. Jang, H. Park, W.Y. Kim, Y.H. Lee, S.H. Choi, J.S. Lee, Carbon dioxide Fischer-Tropsch synthesis: a new path to carbon-neutral fuels, Appl. Catal. B: Environ. 202 (2017) 605–610.
[13] R. Dorner, H. Willauer, D. Hardy, F. Williams, Eff. Load. Doping Iron-Based CO2 Hydrog. Catal. (2009) 18.
[14] T. Riedel, M. Claeys, H. Schulz, G. Schaub, S.-S. Nam, K.-W. Jun, M.-J. Choi, G. Kishan, K.-W. Lee, Comparative study of Fischer–Tropsch synthesis with H2/CO and H2/CO2 syngas using Fe- and Co-based catalysts, Appl. Catal. A: Gen. 186 (1999) 201–213.
[15] K.-W. Jun, S.-J. Lee, H. Kim, M.-J. Choi, K.-W. Lee, Support effects of the promoted and unpromoted iron catalysts in CO2 hydrogenation, in: T. Inui, M. Anpo, K. Izui, S. Yanagida, T. Yamaguchi (Eds.), Stud. Surf. Sci. Catal., Elsevier, 1998, pp. 345–350.
[16] N. Boreriboon, X. Jiang, C. Song, P. Prasassarakich, Higher hydrocarbons synthesis from CO2 hydrogenation over K- and La-promoted Fe–Cu/TiO2 catalysts, Top. Catal. 61 (2018) 1551–1562.
[17] C. Panzone, R. Philippe, A. Chappaz, P. Fongarland, A. Bengaouer, Power-to-Liquid catalytic CO2 valorization into fuels and chemicals: focus on the Fischer-Tropsch route, J. CO2 Util. 38 (2020) 314–347.
[18] A.J. Urquhart, J.M. Keel, F.J. Williams, R.M. Lambert, Electrochemical promotion by potassium of rhodium-catalyzed Fischer−Tropsch synthesis: XP spectroscopy and reaction Studies, J. Phys. Chem. B 107 (2003) 10591–10597.
[19] A. Urquhart, F. Williams, R. Lambert, Electrochemical promotion by potassium of Rh-catalysed Fischer–Tropsch synthesis at high pressure, Catal. Lett. 103 (2005) 137–141.
[20] D. Tsiplakides, S. Balomenou, Milestones and perspectives in electrochemically promoted catalysis, Catal. Today 146 (2009) 312–318.
[21] D. Tsiplakides, S. Balomenou, Electrochemical promoted catalysis: towards practical utilization, Chem. Ind. Chem. Eng. Q 14 (2008) 97–105.
[22] N.A. Anastasijevic, NEMCA—from discovery to technology, Catal. Today 146 (2009) 308–311.
[23] C.G. Vayenas, S. Bebelis, C. Pliangos, S. Brosda, D. Tsiplakides, Electrochemical activation of catalysis: promotion, electrochemical promotion, and metal-support interactions, Kluwer Academic/Plenum Publishers, New York, 2001.
[24] S. Bebelis, H. Karasali, C.G. Vayenas, Electrochemical promotion of the CO2 hydrogenation on Pd/YSZ and Pd/β″-Al2O3 catalyst-electrodes, Solid State Ion. 179 (2008) 1391–1395.
[25] D. Theleritis, M. Makri, S. Souentie, A. Caravaca, A. Katsaounis, C.G. Vayenas, Comparative study of the electrochemical promotion of CO2 hydrogenation over Ru-supported catalysts using electronegative and electropositive promoters, ChemElectroChem 1 (2014) 254–262.
[26] I. Kalaitzidou, M. Makri, D. Theleritis, A. Katsaounis, C.G. Vayenas, Comparative study of the electrochemical promotion of CO2 hydrogenation on Ru using Na+, K+, H+ and O2− conducting solid electrolytes, Surf. Sci. 646 (2016) 194–203.
[27] J. Díez-Ramírez, P. Sánchez, J.L. Valverde, F. Dorado, Electrochemical promotion and characterization of PdZn alloy catalysts with K and Na ionic conductors for pure gaseous CO2 hydrogenation, J. CO2 Util. 16 (2016) 375–383.
[28] M. Makri, A. Katsaounis, C.G. Vayenas, Electrochemical promotion of CO2 hydrogenation on Ru catalyst–electrodes supported on a K–β″–Al2O3 solid electrolyte, Electrochim. Acta 179 (2015) 556–564.
[29] N. Gutiérrez-Guerra, J. González-Cobos, J.C. Serrano-Ruiz, J.L. Valverde, A. de Lucas-Consuegra, Electrochemical activation of Ni catalysts with potassium ionic conductors for CO2 hydrogenation, Top. Catal. 58 (2015) 1256–1269.
[30] C. Panaritis, M. Edake, M. Couillard, R. Einakchi, E.A. Baranova, Insight towards the role of ceria-based supports for reverse water gas shift reaction over RuFe nanoparticles, J. CO2 Util. 26 (2018) 350–358.
[31] C. Panaritis, J. Zgheib, M. Couillard, E.A. Baranova, The role of Ru clusters in Fe carbide suppression for the reverse water gas shift reaction over electropromoted Ru/FeOx catalysts, Electrochem. Commun. 119 (2020) 106824.
[32] C. Panaritis, J. Zgheib, S.A.H. Ebrahim, M. Couillard, E.A. Baranova, Electrochemical in-situ activation of Fe-oxide nanowires for the reverse water gas shift reaction, Appl. Catal., B 269 (2020) 118826.
[33] C. Panaritis, S. Yan, M. Couillard, E.A. Baranova, Electrochemical study of the metal-support interaction between FeOx nanoparticles and cobalt oxide support for the reverse water gas shift reaction, J. CO2 Util. 56 (2022) 101824.
[34] F. Williams, R. Lambert, A study of sodium promotion in Fischer-Tropsch synthesis: electrochemical control of a ruthenium model catalyst, Catal. Lett. 70 (2000).
[35] E. Ruiz, D. Cillero, P.J. Martínez, Á. Morales, G.S. Vicente, G. de Diego, J. M. Sánchez, Electrochemical synthesis of fuels by CO2 hydrogenation on Cu in a potassium ion conducting membrane reactor at bench scale, Catal. Today 236 (2014) 108–120.
[36] E. Ruiz, D. Cillero, P.J. Martínez, Á. Morales, G.S. Vicente, G. de Diego, J. M. Sánchez, Bench-scale study of electrochemically assisted catalytic CO2 hydrogenation to hydrocarbon fuels on Pt, Ni and Pd films deposited on YSZ, J. CO2 Util. 8 (2014) 1–20.
[37] E. Ruiz, P.J. Martínez, Á. Morales, G. San Vicente, G. de Diego, J.M. Sánchez, Electrochemically assisted synthesis of fuels by CO2 hydrogenation over Fe in a bench scale solid electrolyte membrane reactor, Catal. Today 268 (2016) 46–59.
[38] E. Ruiz, D. Cillero, P.J. Martínez, Á. Morales, G.S. Vicente, G. de Diego, J. M. Sánchez, Bench scale study of electrochemically promoted catalytic CO2 hydrogenation to renewable fuels, Catal. Today 210 (2013) 55–66.
[39] E. Ruiz, J. Aldecoa, Á. Morales, M. Farchado, J.M. Sánchez, Methanation of CO2 on Cu in a tubular co-ionic SOEC, Int. J. Hydrog. Energy 52 (2024) 1338–1359.
[40] Y. Hajar, V. Di Palma, V. Kyriakou, M.A. Verheijen, E.A. Baranova, P. Vernoux, W. M.M. Kessels, M. Creatore, M.C.M. van de Sanden, M.N. Tsampas, Atomic layer deposition of highly dispersed Pt nanoparticles on a high surface area electrode backbone for electrochemical promotion of catalysis, Electrochem. Commun. 84 (2017) 40–44.

[41] E.I. Papaioannou, S. Souentie, A. Hammad, C.G. Vayenas, Electrochemical promotion of the CO2 hydrogenation reaction using thin Rh, Pt and Cu films in a monolithic reactor at atmospheric pressure, Catal. Today 146 (2009) 336–344.
[42] D. Theleritis, S. Souentie, A. Siokou, A. Katsaounis, C.G. Vayenas, Hydrogenation of CO2 over Ru/YSZ electropromoted catalysts, ACS Catal. 2 (2012) 770–780.
[43] A. Morales, EU EP 1 321 539 A2.
[44] R.B. Unde, Kinetics and Reaction Engineering Aspects of Syngas Production by the Heterogeneously Catalysed Reverse Water Gas Shift Reaction, Ph.D. Thesis, University of Bayreuth, 2012.
[45] P.H. Choi, K.-W. Jun, S.-J. Lee, M.-J. Choi, K.-W. Lee, Hydrogenation of carbon dioxide over alumina supported Fe-K catalysts, Catal. Lett. 40 (1996) 115–118.
[46] M. Maroño, J.M. Sánchez, E. Ruiz, A. Cabanillas, Study of the suitability of a pt-based catalyst for the upgrading of a biomass gasification syngas stream via the WGS reaction, Catal. Lett. 126 (2008) 396–406.
[47] M. Maroño, J.M. Sánchez, E. Ruiz, Hydrogen-rich gas production from oxygen pressurized gasification of biomass using a Fe–Cr Water Gas Shift catalyst, Int. J. Hydrog. Energy 35 (2010) 37–45.
[48] P. Munnik, P.E. de Jongh, K.P. de Jong, Recent developments in the synthesis of supported catalysts, Chem. Rev. 115 (2015) 6687–6718.
[49] W. Du, S. Yang, F. Pan, J. Shangguan, J. Lu, S. Liu, H. Fan, Hydrogen reduction of hematite ore fines to magnetite ore fines at low temperatures, J. Chem. 2017 (2017) 1919720.
[50] A.V. Puga, On the nature of active phases and sites in CO and CO2 hydrogenation catalysts, Catal. Sci. Technol. 8 (2018) 5681–5707.
[51] W.K. Jozwiak, E. Kaczmarek, T.P. Maniecki, W. Ignaczak, W. Maniukiewicz, Reduction behavior of iron oxides in hydrogen and carbon monoxide atmospheres, Appl. Catal. A: Gen. 326 (2007) 17–27.
[52] L. Niu, X. Liu, X. Wen, Y. Yang, J. Xu, Y. Li, Effect of potassium promoter on phase transformation during H2 pretreatment of a Fe2O3 Fischer Tropsch synthesis catalyst precursor, Catal. Today 343 (2020) 101–111.
[53] N. Fischer, R. Henkel, B. Hettel, M. Iglesias, G. Schaub, M. Claeys, Hydrocarbons via CO2 hydrogenation over iron catalysts: the effect of potassium on structure and performance, Catal. Lett. 146 (2016) 509–517.
[54] G. Bergeret, P. Gallezot, Particle size and dispersion measurements. Handbook of Heretogeneous Catalysis, Wiley-VCH, 2008, pp. 738–765.
[55] T. Xie, J. Wang, F. Ding, A. Zhang, W. Li, X. Guo, C. Song, CO2 hydrogenation to hydrocarbons over alumina-supported iron catalyst: effect of support pore size, J. CO2 Util. 19 (2017) 202–208.
[56] B. Yao, T. Xiao, O.A. Makgae, X. Jie, S. Gonzalez-Cortes, S. Guan, A.I. Kirkland, J. R. Dilworth, H.A. Al-Megren, S.M. Alshihri, P.J. Dobson, G.P. Owen, J.M. Thomas, P.P. Edwards, Transforming carbon dioxide into jet fuel using an organic combustion-synthesized Fe-Mn-K catalyst, Nat. Commun. 11 (2020) 6395.
[57] M.V. Landau, N. Meiri, N. Utsis, R. Vidruk Nehemya, M. Herskowitz, Conversion of CO2, CO, and H2 in CO2 hydrogenation to fungible liquid fuels on Fe-based catalysts, Ind. Eng. Chem. Res. 56 (2017) 13334–13355.
[58] S. Choi, B.-I. Sang, J. Hong, K.J. Yoon, J.-W. Son, J.-H. Lee, B.-K. Kim, H. Kim, Catalytic behavior of metal catalysts in high-temperature RWGS reaction: In-situ FT-IR experiments and first-principles calculations, Sci. Rep. 7 (2017) 41207.
[59] S. Saeidi, N.A.S. Amin, M.R. Rahimpour, Hydrogenation of CO2 to value-added products—a review and potential future developments, J. CO2 Util. 5 (2014) 66–81.
[60] H. Schulz, T. Riedel, G. Schaub, Fischer–Tropsch principles of co-hydrogenation on iron catalysts, Top. Catal. 32 (2005) 117–124.
[61] M. Niemelä, M. Nokkosmäki, Activation of carbon dioxide on Fe-catalysts, Catal. Today 100 (2005) 269–274.
[62] D. Miller, M. Moskovits, Separate pathways for oxygenate and hydrocarbon synthesis in the Fischer-Tropsch reaction, J. Am. Chem. Soc. 111 (1989) 9250–9252.
[63] H. Kusama, K. Okabe, K. Sayama, H. Arakawa, Ethanol synthesis by catalytic hydrogenation of CO2 over RhFeSiO2 catalysts, Energy 22 (1997) 343–348.
[64] W. Ma, E.L. Kugler, D.B. Dadyburjor, Potassium effects on activated-carbon-supported iron catalysts for fischer-tropsch synthesis, Energy Fuels 21 (2007) 1832–1842.
[65] Q. Wang, K. Hu, R. Gao, L. Zhang, L. Wang, C. Zhang, Hydrogenation of carbon dioxide to value-added liquid fuels and aromatics over fe-based catalysts based on the fischer–tropsch synthesis route, Atmosphere 13 (2022) 1238.
[66] C. Finnerty, G.A. Tompsett, K. Kendall, R.M. Ormerod, SOFC system with integrated catalytic fuel processing, J. Power Sources 86 (2000) 459–463.
[67] N.B. Jackson, L. Evans, A. Datye, Attrition-determining morphology changes on iron Fischer-Tropsch catalysts, in: A. Parmaliana, D. Sanfilippo, F. Frusteri, A. Vaccari, F. Arena (Eds.), Studies in Surface Science and Catalysis, Elsevier, 1998, pp. 137–142.
[68] X. Yao, Q. Yu, Z. Ji, Y. Lv, Y. Cao, C. Tang, F. Gao, L. Dong, Y. Chen, A comparative study of different doped metal cations on the reduction, adsorption and activity of CuO/Ce0. 67M0. 33O2 (M= Zr4+, Sn4+, Ti4+) catalysts for NO+ CO reaction, Appl. Catal., B 130 (2013) 293–304.
[69] L. Dai, Y. Chen, R. Liu, X. Li, N. Ullah, Z. Li, CO2 hydrogenation to C5+ hydrocarbons over K-promoted Fe/CNT catalyst: Effect of potassium on structure–activity relationship, Appl. Organomet. Chem. 35 (2021) e6253.